RESEARCH ARTICLE

Serotonergic modulation of visual neurons in *Drosophila melanogaster*

Maureen M. Sampson[1,2☉], **Katherine M. Myers Gschweng**[1,3☉], **Ben J. Hardcastle**[4], **Shivan L. Bonanno**[1,3], **Tyler R. Sizemore**[5], **Rebecca C. Arnold**[1,3], **Fuying Gao**[3], **Andrew M. Dacks**[5], **Mark A. Frye**[4], **David E. Krantz**[1,3]*

1 UCLA, Hatos Center for Neuropharmacology, Los Angeles, CA, United States of America, **2** UCLA, Molecular Toxicology Interdepartmental Program, Los Angeles, CA, United States of America, **3** UCLA, Department of Psychiatry and Biobehavioral Sciences, Semel Institute for Neuroscience and Human Behavior, David Geffen School of Medicine, Los Angeles, CA, United States of America, **4** UCLA, Department of Integrative Biology and Physiology, Los Angeles, CA, United States of America, **5** Department of Biology, West Virginia University, Morgantown, WV, United States of America

☉ These authors contributed equally to this work.
* dkrantz@ucla.edu

Abstract

Sensory systems rely on neuromodulators, such as serotonin, to provide flexibility for information processing as stimuli vary, such as light intensity throughout the day. Serotonergic neurons broadly innervate the optic ganglia of *Drosophila melanogaster*, a widely used model for studying vision. It remains unclear whether serotonin modulates the physiology of interneurons in the optic ganglia. To address this question, we first mapped the expression patterns of serotonin receptors in the visual system, focusing on a subset of cells with processes in the first optic ganglion, the lamina. Serotonin receptor expression was found in several types of columnar cells in the lamina including 5-HT2B in lamina monopolar cell L2, required for spatiotemporal luminance contrast, and both 5-HT1A and 5-HT1B in T1 cells, whose function is unknown. Subcellular mapping with GFP-tagged 5-HT2B and 5-HT1A constructs indicated that these receptors localize to layer M2 of the medulla, proximal to serotonergic boutons, suggesting that the medulla neuropil is the primary site of serotonergic regulation for these neurons. Exogenous serotonin increased basal intracellular calcium in L2 terminals in layer M2 and modestly decreased the duration of visually induced calcium transients in L2 neurons following repeated dark flashes, but otherwise did not alter the calcium transients. Flies without functional 5-HT2B failed to show an increase in basal calcium in response to serotonin. 5-HT2B mutants also failed to show a change in amplitude in their response to repeated light flashes but other calcium transient parameters were relatively unaffected. While we did not detect serotonin receptor expression in L1 neurons, they, like L2, underwent serotonin-induced changes in basal calcium, presumably via interactions with other cells. These data demonstrate that serotonin modulates the physiology of interneurons involved in early visual processing in *Drosophila*.

Author summary

Serotonergic neurons innervate the *Drosophila melanogaster* eye, but it was not known whether serotonin signaling could induce acute physiological responses in visual interneurons. We found serotonin receptors expressed in all neuropils of the optic lobe and identified specific neurons involved in visual information processing that express serotonin receptors. Activation of these receptors increased intracellular calcium in first order interneurons L1 and L2 and may enhance visually induced calcium transients in L2 neurons. These data support a role for the serotonergic neuromodulation of interneurons in the *Drosophila* visual system.

Introduction

Serotonin acts as a neuromodulator [1–5] in a variety of networks including the sensory systems required for olfaction, hearing, and vision [6–17]. In the mammalian visual cortex, serotonin regulates the balance of excitation and inhibition [6], cellular plasticity [18–21], and response gain [8, 22]. In some cases, the contribution of individual receptor subtypes is known; for example, in the mammalian retina, serotonergic signaling reduces GABAergic amacrine cell input to retinal ganglion cells via 5-HT1A [23]. Additionally, some retinal ganglion cells express 5-HT2C and loss of this receptor enhanced the response to contrast-reversing gratings [24]. However, for most sensory circuits, the manner in which serotonin receptor activation is integrated to regulate their activity and drive adaptive changes remains poorly understood.

The visual system of *Drosophila melanogaster* provides a genetically tractable model to study visual circuit activity and regulation [25,26]. In *Drosophila*, early visual processing occurs in the lamina where intrinsic monopolar neurons receive direct input from photoreceptors [27]. Lamina monopolar cells L1 and L2 are first-order interneurons that feed into pathways discriminating light "ON" (i.e., increase in luminance) and light "OFF" (i.e., decrease in luminance) stimuli respectively [28,29]. L1 and L2 neurons respond to changes in luminance in a physiologically indistinguishable manner [30–32], while downstream neurons in the medulla transform this information to discriminate ON versus OFF stimuli [29]. Further processing occurs in the lobula and lobula plate to mediate higher-order computations for both motion and contrast detection [29,33,34]. Significant progress has been made in mapping the synaptic connectivity and function of visual processing neurons, including those required for motion detection [27,35–40].

Additional studies have shown that aminergic neurotransmitters can modulate visual information processing in flies and other insects [26,41–46]. Octopamine, the invertebrate equivalent of noradrenaline, is present in processes innervating the medulla, lobula and lobula plate in *Drosophila*, where it regulates state-dependent modulation of visual interneurons [42,46] including the saliency of objects during flight [43]. Serotonergic neurons also innervate the optic ganglia [47–52] and previous studies indicate that serotonin impacts cellular activity and visual behaviors in insects [44,45,53–56]. In *Drosophila*, serotonin was shown to modulate the voltage dependence of potassium channels in photoreceptors [44]. In the blowfly, serotonin alters electrophysiological field recordings representing the combined output of lamina neurons [53]. In the honeybee, single cell recordings in motion-sensitive lobula neurons showed that serotonergic signaling reduces background activity, directional selectivity, and the amplitude of field potentials evoked by moving stripes [45].

The visual system is also essential for setting and maintaining circadian rhythms [57,58]. Physiological changes in photoreceptors and downstream interneurons may facilitate adaptation to circadian changes in light intensity or other stimuli. In houseflies, serotonin and other neurotransmitters regulate daily rhythmic swelling of monopolar cell L2 terminals in the medulla [59], a process that was proposed to decrease monopolar signal in the daytime when light levels increase. In *Drosophila*, serotonin levels decrease in constant darkness [56], possibly correlating with changes in photosensory input and contributing to adaptation to varying light levels throughout the day. In contrast, serotonin levels increase during the dark phase in the sphinx moth [9] and cricket [60]. Serotonin also regulates circadian behaviors in *Drosophila* [55,56], but the potential contributions of specific subtypes of serotonin receptors to circadian processes or more acute changes in the visual environment remains unclear.

Serotonin receptor signaling occurs via diverse secondary messenger cascades [61,62] and receptors may act individually or in combination within a single cell [63,64] or circuit [65]. Co-activation of both 5-HT1A and 5-HT2A in cortical pyramidal neurons leads to complex physiologic responses [65,66] that are further regulated by 5HT1A receptors on local inhibitory neurons [67]. The effects of receptor activation can also vary depending on inputs from other neuromodulators [68] and the differential activation of downstream effectors [65,69]. These studies highlight the difficulties of predicting the effects of serotonin receptor activation based solely on expression data, and the need for physiological assays to assess their role in specific circuits. Although two recent studies have reported serotonin receptor expression in visual neurons [70,71], to our knowledge there is no information on the physiological effect(s) of any serotonin receptor in any of the interneurons within the insect visual system. In this work, we show how a specific serotonin receptor, 5-HT2B, affects intracellular calcium and visual responses in L2 lamina monopolar cells, which are critical for early visual information processing.

Results

Distinct lamina neurons express different serotonin receptors

Five genes encoding serotonin receptors have been identified in the *Drosophila* genome: 5-HT1A, 5-HT1B, 5-HT2A, 5-HT2B and 5-HT7 [72–76]. To identify specific optic lobe neurons expressing each receptor, we expressed the marker mCD8::RFP (or GFP) under the control of a recently characterized panel of T2A-GAL4 insertions in Minos-Mediated Integration Cassettes (MiMICs) located in serotonin receptor gene introns [77]. The GAL4 sequence is inserted into receptor-encoding genes where it acts as an artificial exon and is expected to "mimic" the endogenous gene expression patterns [78]. Ribosome skipping via T2A allows GAL4 to be expressed as a separate protein, rather than a fusion protein with the serotonin receptor [77,79].

We observed distinct expression patterns for each receptor including projections into the optic lobe neuropils: the lamina (la), medulla (me), lobula (lo) and lobula plate (lp) (S1 Fig). We focus here on receptor subtypes showing expression in the lamina because of the ease of identifying cells based on their morphology [80], the established role of some lamina neurons in the response to experimentally tractable visual stimuli [28,29,81], and the proposed relationship between serotonin and circadian changes in a subset of lamina neurons in larger flies [59].

To identify the specific cell types that express each serotonin receptor in the lamina, we used the receptor MiMIC-T2A-GAL4 lines described above in combination with the sparse labeling technique MultiColor FlpOut 1 (MCFO) [82]. Using 5-HT1A and 5-HT1B MiMIC-T2A-GAL4 lines with MCFO we frequently observed a cell with a soma in the medulla cortex,
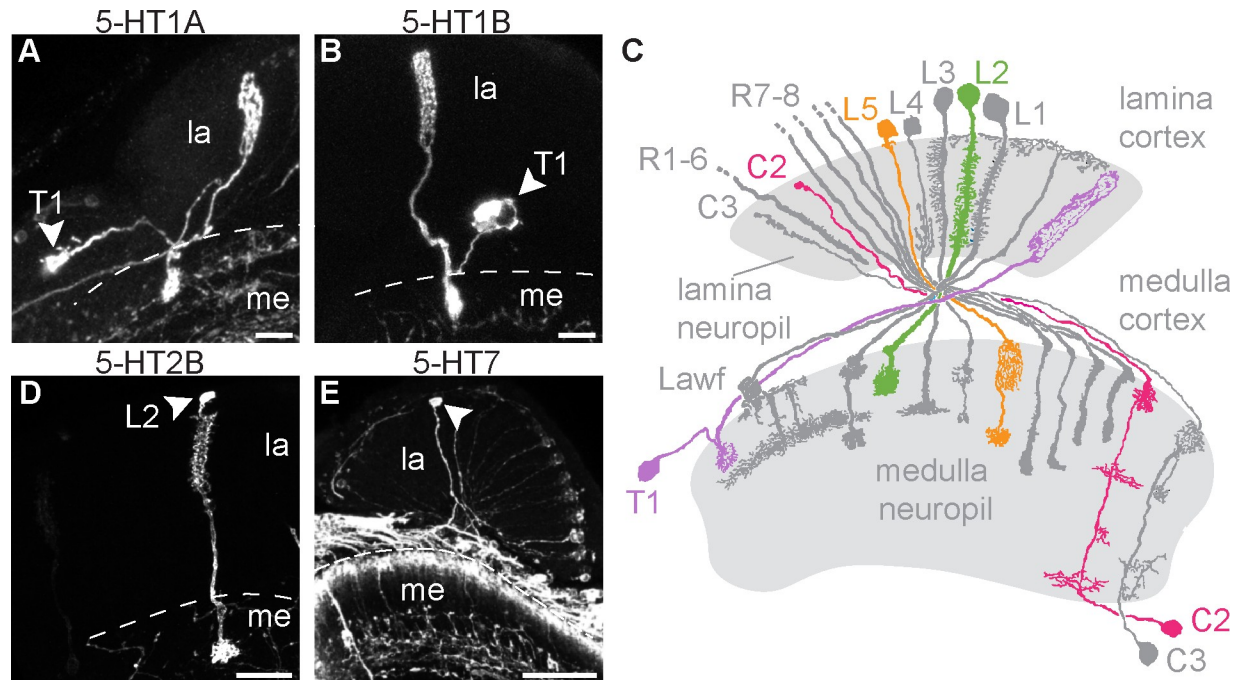
Fig 1. Lamina neurons including T1 and L2 express serotonin receptors. (A-E) Serotonin receptor MiMIC-T2A-GAL4 lines were crossed to UAS-MCFO-1 to sparsely label individual cells in the lamina. Cell bodies are indicated by an arrowhead. 5-HT1A (**A**) and 5-HT1B (**B**) MCFO crosses revealed cells with morphologies identical to T1 neurons. (**C**) A diagram showing lamina neurons adapted from [80] highlights L2 (green), L5 (orange), T1 (purple), and C2 (pink). (**D**) 5-HT2B>MCFO labeled cells were morphologically identical to L2 neurons. (**E**) 5-HT7>MCFO-1 labeled neurons possibly representing L5 lamina monopolar cells. Scale bars are 20 μm and N = 9–31 brains imaged per receptor subtype. Due to the nature of stochastic labeling, some cell types were observed in only a subset of brains: 22/31 (**A**), 10/11 (**B**), 9/9 (**D**), and 7/13 (**E**).

a long basket-like projection in the lamina, and a smaller projection in the medulla (Fig 1A and 1B). This morphology is identical to that of T1 cells and distinct from other cell types in the lamina (Fig 1C) [80]. T1 cells were labeled in 23 of 31 brains (71%) for 5-HT1A and in 10 of 11 brains (91%) for 5-HT1B. On average, we observed thirteen MCFO-labeled T1 cells per individual optic lobe for 5-HT1A and nine T1 cells per optic lobe for 5-HT1B. These data are consistent with the results of recently published studies that used TAPIN-Seq or FACS-S-MART-Seq to analyze expression in T1 as well as other cells in the visual system [70,71] (see S2 Fig for a comparison of these findings).

Using the 5-HT2B MiMIC-T2A-GAL4 driver with MCFO, we observed cells with a soma in the lamina cortex, dense projections extending into the lamina neuropil, and a single bushy terminal in the medulla (Fig 1D), together representing a morphology identical to lamina monopolar neuron L2 and no other lamina cell types (Fig 1C) [80]. We observed L2 cells in 9 of 9 (100%) 5-HT2B>MCFO brains, observing an average of eleven L2 neurons per optic lobe. Additionally, we co-expressed 5-HT2B>RFP with MiMIC-T2A-Lex-ChAT>GFP and found that a subset of the lamina monopolar cells co-labeled with both lines, consistent with the neurochemical identity of L2 cells as cholinergic (S3A Fig, arrowheads).

For 5-HT7>MCFO, we observed lamina monopolar cells in 7 of 13 brains (54%) (Fig 1E), with an average of 20 cells per optic lobe. Over 99% of the lamina monopolar cells labeled with 5-HT7>MCFO lacked the dense processes in the lamina neuropil that are characteristic of L1-L3, and also lacked the vertically oriented collaterals in the inner (proximal) lamina seen in L4 neurons (Fig 1C and 1E). We therefore suggest that 5-HT7 may be expressed in the one

remaining lamina monopolar cell subtype, L5. Additional examples of 5-HT7>MCFO labeled cells possibly representing L5 are included in S3B and S3C Fig.

We detected additional, less frequent events for other columnar cells in the lamina. These include observations of multiple centrifugal cells (C2 or C3) in 3 of 31 5-HT1A>MCFO brains (S3D Fig) consistent with two previous reports of 5-HT1A in C2 [70, 71]. In further support of the expression of 5-HT1A in centrifugal cells, we observed co-expression of 5-HT1A>RFP and MiMIC-LexA GAD1>GFP in thin projections in the lamina and in cell bodies between the proximal medulla cortex and the lobula plate (S2E Fig, arrowheads).

Medulla neurons, glia and serotonergic neurons express serotonin receptors

The results of other more comprehensive studies of RNA expression in visual system neurons prompted us to look beyond our primary focus of lamina neurons [70,71]. In addition to the columnar neurons that express serotonin receptors and extend projections into the lamina [80], we have tentatively identified cells with projections that are either confined to the medulla, or include both medulla and lobula complex, and may also express serotonin receptors (S3F–S3H Fig).

For 5-HT2A>MCFO, additional pleomorphic labeling was observed in the lamina cortex (S4A Fig) in a pattern that appeared similar to that of optic lobe glia [83]. Anti-repo labeled nuclei showed close proximity to many 5-HT2A labeled cells (S4B Fig), but one-to-one matching was not possible due to irregular cell morphology. A previous microarray study of glia suggested that 5-HT1A and 5-HT7 are enriched in repo-GAL4 specified glia, while 5-HT1B was enriched in surface glia [84]. Another previous study [70] reported expression of 5-HT7 in three types of lamina glia—epithelial glia, proximal satellite glia and marginal glia.

The major ganglia of the visual system do not contain any serotonergic cell bodies; rather projections from neurons in the accessory medulla and central brain innervate the optic lobes [50,85–88]. We observed a cluster of 8–10 cell bodies in the accessory medulla (S5A Fig, S5C Fig) that corresponds to cluster LP2 (or Cb1), which was previously reported to project into the medulla [85]. Additionally, two symmetric, serotonin-immunoreactive neurons designated LBO5HT have cell bodies in the ventral protocerebrum and bilaterally innervate the lamina, medulla, lobula and lobula plate [85]. Immunolabeling for serotonergic boutons can be observed within all optic ganglia neuropil as well as the lamina cortex (S5A Fig) [50,85–88]; e.g. arborizations from 5-HT1B>GFP labeled cells in the outer medulla, which we have identified as T1 projections, were surrounded by a honeycomb pattern of serotonergic immunolabeling (S5C Fig).

Sparse labeling with 5-HT1B>MCFO co-labeled with serotonin-immunolabeled boutons in the inner medulla (iM), medulla layer 4 (M4), and lobula (lo) (S5E Fig), suggesting that 5-HT1B could function as an autoreceptor in these processes. Previous studies have also reported 5-HT1B and 5-HT1A as potential autoreceptors in *Drosophila* [56,89]. Although we did not comprehensively map all putative serotonin autoreceptors in the central brain, we used serotonergic cell maps described in [50,85,87,88] to identify 5-HT1B+ cell clusters as LP2 (Cb1), PLP (LP1), and PMP, (S5 Fig) and 5-HT1A+ serotonergic clusters as PLP (LP1), SEL, AMP and PMP (S6 Fig). The integration of physiological studies in both serotonergic neurons and post-synaptic neurons represents a future goal to assess the interplay between auto- and post-synaptic receptors in visual circuits.

L2 neurons express 5-HT2B and T1 neurons express 5-HT1A and 5HT1B

We sought to confirm the expression of serotonin receptors independently of both previous studies [70,71] and the data we obtained using MiMIC-T2A-GAL4 lines. To this end, we used
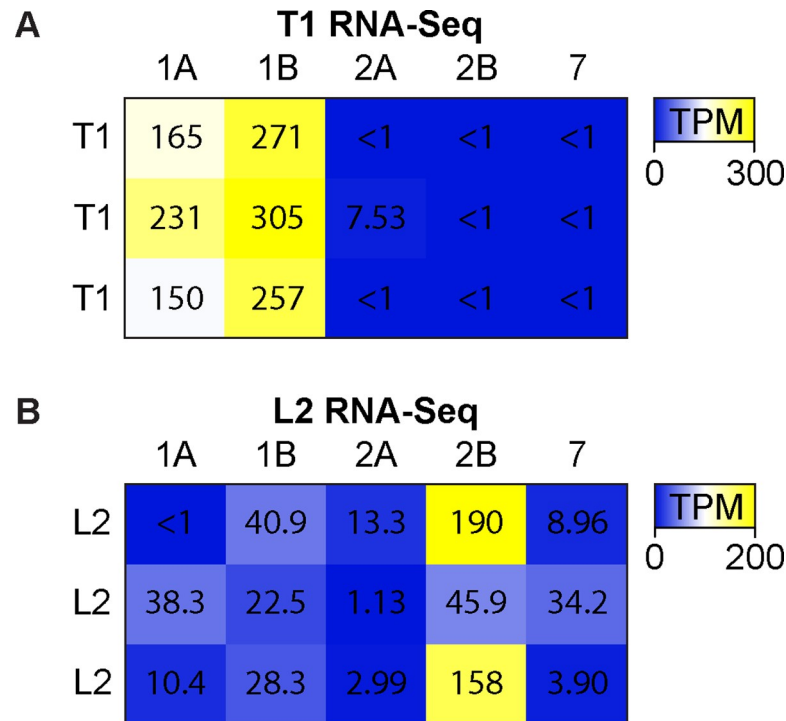
a separate set of split-GAL4 [90] or LexA drivers previously shown to be specific for particular cell types, and focused on a small subset of lamina neurons: T1, L1 and L2. Drivers representing each cell were used to express GFP, and the GFP-labeled cells were isolated via Fluorescence Activated Cell Sorting (FACS). RNA was then extracted from T1, L1 and L2 GFP + FACS isolates as well as the unlabeled cells. To probe for serotonin receptor expression in each cell type, we used both RNA-Seq (Fig 2 and S1 Table) and RT-qPCR (S7 Fig and S2 Table).

For RNA-Seq, we compared the relative abundance for each receptor by calculating Transcripts Per Kilobase Millions (TPMs). We found that 5-HT1A (182±43 TPM±std) and 5-HT1B (278±25 TPM±std) were more abundant than other serotonin receptors (range 0.01 ±0.01 to 2.5±4 TPM±std) in T1 samples (N = 3, Fig 2A and S1 Table). Two previous sequencing studies similarly reported the expression of 5-HT1A and 5-HT1B in T1 [70,71]. L2 isolates showed higher TPMs for 5-HT2B (130±75 TPM±std) compared to other serotonin receptors (range 6±7 to 31±9 TPM±std) (Fig 2B and S1 Table), also consistent with the results of another recent transcriptomic study [70]. For RT-qPCR, we calculated enrichment (i.e., fold change) relative to pooled, unlabeled optic lobe cells using the comparative CT method [91]. Relative to unlabeled optic lobe neurons, L2 samples were enriched for 5-HT2B in 4/5 samples but also showed enrichment for 5-HT7 and 5-HT2A in 3/5 and 1/5 samples respectively (S7 Fig and S2 Table). Although we cannot rule out the presence of 5-HT2A or 5-HT7 in L2 based on the results of RT-qPCR, our data and those of others [70] suggest that 5-HT2B may be the only serotonin receptor abundantly expressed in L2 cells.

We did not observe evidence of any serotonin receptor expression in L1 neurons using the serotonin receptor MiMIC-T2A-GAL4 lines to drive MCFO. In agreement with this observation, RT-qPCR from isolated L1 cells (S7 Fig and S1 Table) showed virtually no receptor expression, apart from one sample weakly enriched for 5-HT1B. Others have also reported a low likelihood of any serotonin receptor expression in L1 neurons [70]. In sum, MCFO sparse labeling in combination with RNA-Seq and RT-qPCR by our group and others [70,71] indicate that T1 neurons express 5-HT1A and 5-HT1B, and L2 neurons express 5-HT2B, whereas L1 neurons may not express any serotonin receptor subtypes.

5-HT2B and 5-HT1A receptors localize to the medulla neuropil

Both T1 and L2 neurons have dense projections in the lamina neuropil and arborize in layer 2 (M2) of the medulla neuropil. Serotonergic neurons directly innervate M1 and M2 of the medulla neuropil raising the possibility that serotonergic signaling might occur at this site. If so, we reasoned that the serotonin receptors expressed in L2 and T1 might localize to M1 and/ or M2. To test this possibility, we took advantage of a 5-HT1A allele that had been tagged at the C-terminus with GFP [92]. The tag was inserted into the endogenous 5-HT1A gene, such that, similar to MiMIC-T2A-GAL4 lines [77, 78], the receptor::GFP fusion protein product is putatively expressed at the same level and in the same cells as the endogenous protein [92]. In 5-HT1A::GFP flies, we observed enrichment of the tagged protein in layer M2 of the medulla relative to other subcellular sites (Fig 3A–3A"), suggesting that serotonergic signaling to 5-HT1A::GFP expressing neurons occurs in this region. This might include T1 as well as other columnar neurons that extend processes into M2. Regardless of cell type, there is very low 5-HT1A::GFP signal in the lamina neuropil (Fig 3A'), suggesting that serotonergic signaling primarily targets 5-HT1A receptors localized to the medulla neuropil. We also observed anti-serotonin immunoreactive puncta that co-labeled with 5-HT1A::GFP in the medulla suggesting that 5-HT1A could act as an autoreceptor in serotonergic projection neurons innervating the medulla (Fig 3B, arrows, and S6 Fig).

A T1 RNA-Seq

	1A	1B	2A	2B	7
T1	165	271	<1	<1	<1
T1	231	305	7.53	<1	<1
T1	150	257	<1	<1	<1

TPM
0   300

B L2 RNA-Seq

|	1A	1B	2A	2B	7
L2	<1	40.9	13.3	190	8.96
L2	38.3	22.5	1.13	45.9	34.2
L2	10.4	28.3	2.99	158	3.90

TPM
0   200

Fig 2. L2 neurons express 5-HT2B and T1 neurons express both 5-HT1A and 5-HT1B serotonin receptors. T1 or L2 neurons were isolated by FACS for RNA-Seq. Transcript abundance was calculated as Transcripts Per Kilobase Million (TPMs). (**A**) T1 RNA-Seq TPMs (color low to high, blue to yellow) were higher for 5-HT1A and 5-HT1B compared to other serotonin receptors. (**B**) L2 RNA-Seq showed high abundance 5-HT2B in two of three samples, with 5-HT2B being the most abundant serotonin receptor transcript in all replicates.

https://doi.org/10.1371/journal.pgen.1009003.g002

Since we were unable to obtain an endogenously tagged allele of 5-HT2B, we relied on expression of the UAS-5-HT2B::sfGFP transgene [93] under the control of L2-split-GAL4 to investigate its subcellular localization (Fig 3C). 5-HT2B::sfGFP was enriched in terminals within M2 of the medulla as compared to the lamina neuropil (Fig 3C–3C") and showed additional punctate labeling in L2 cell bodies (Fig 3C', arrowhead). To control for the possibility that all membrane-bound proteins might appear to be enriched in M2, we expressed the plasma membrane marker UAS-mCD8::GFP using the same L2-split-GAL4 driver. In contrast to 5-HT2B::sfGFP, labeling with mCD8::GFP was most prominent in the cell body and proximal processes with progressively weaker labeling through the lamina and medulla neuropil and no enrichment in layer M2 (Fig 3D"). These data strongly suggest that both 5-HT2B and 5-HT1A preferentially localize to the terminals of L2 and T1 respectively in the medulla layer M2 rather than the lamina neuropil. Serotonergic boutons also localize to several layers within the medulla neuropil but are not found in the lamina neuropil (see S5A Fig). It is therefore more likely that T1 and L2 neurons receive serotonergic signals in the medulla rather than the lamina. This may occur in M2, although we cannot rule out other sites in the medulla where serotonergic boutons are present, but the receptors are less enriched.

To further explore serotonergic signaling to L2 and T1 in the medulla, we used sybGRASP to probe for potential synaptic connections between serotonergic boutons in M2 and the terminals of L2 and T1 [94]. We used the previously established ultrastructural connectivity of L2 onto T1 neurons in the medulla [37,38] as a positive control to validate the use of sybGRASP in detecting interactions within M2, and obtained a robust signal (S8A Fig). By contrast, we did not detect a signal in M2 in sybGRASP experiments in which the serotonergic neurons
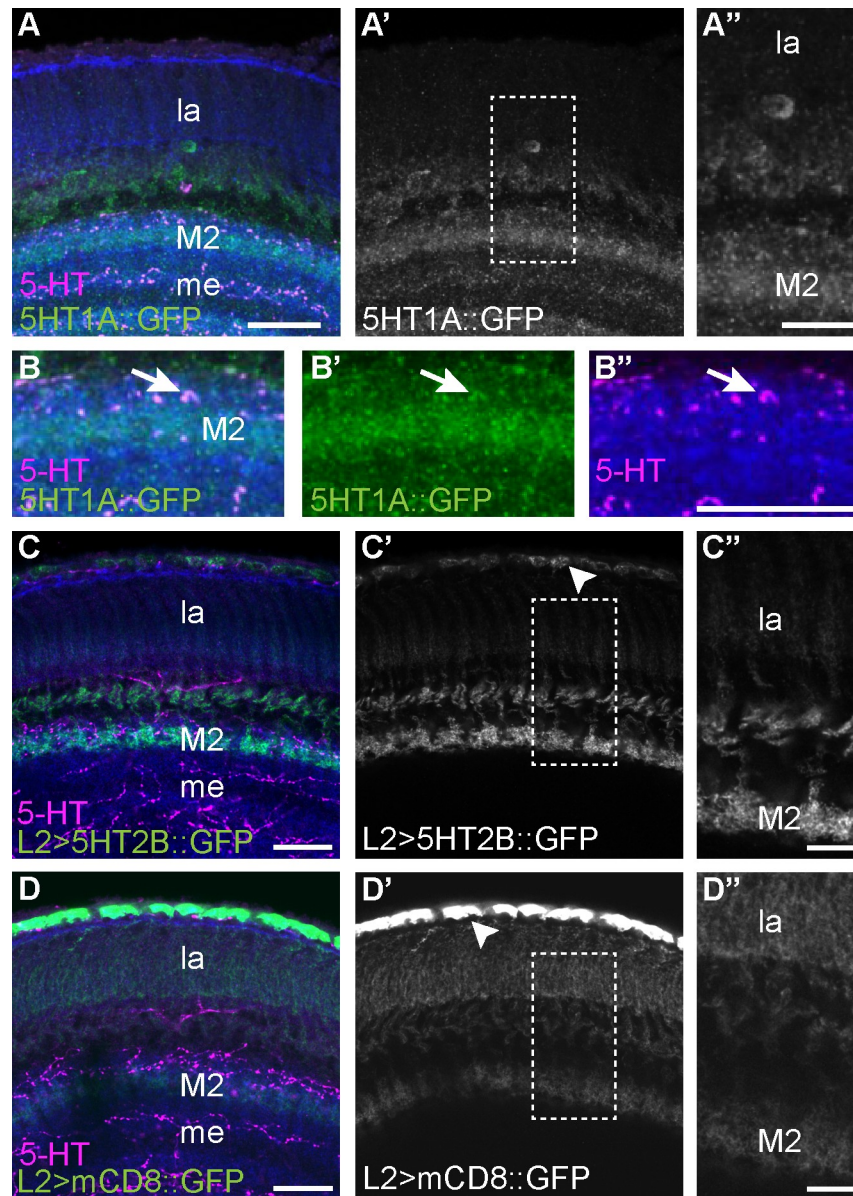
Fig 3. Serotonin receptors 5-HT1A and 5-HT2B are enriched in layer M2 of the medulla. (**A-A"**) 5-HT1A::GFP localized to layer M2 of the medulla, adjacent to some of the boutons in the medulla neuropil immunogenic for serotonin. Neuropil (anti-N-Cadherin, blue) and serotonin (magenta) labeling provide anatomical context for the lamina (la) and medulla (me). The region specified by the dotted lines in (**A'**) is enlarged in (**A"**). (**B-B"**) In some cases, serotonin immunoreactive boutons appeared to be co-labeled rather than adjacent to 5-HT1A::GFP (arrow) possibly representing projections from serotonergic neurons in the central brain. (**C-C"**) Subcellular localization of 5-HT2B was visualized by expressing the fusion construct UAS-5-HT2B::sfGFP in L2 neurons specified by L2-split-Gal4. L2>5-HT2B::sfGFP labeling was stronger in the L2 terminals in medulla layer 2 (M2) compared to L2 projections in the lamina (la). Punctate GFP signal was observed in the L2 cell bodies (arrowhead). The region specified by the dotted lines in (**C'**) is enlarged in (**C"**). (**D-D"**) For comparison, membrane-directed UAS-mCD8::GFP was expressed in L2 neurons. L2>mCD8::GFP signal was similar in the medulla and lamina compartments. Strong GFP signal was observed in the cell bodies (arrowhead). The area within the dotted lines in (**D'**) is enlarged in (**D"**). Scale bars are 20 μm in **A-A'**, **B-B"**, **C-C'** and **D-D'**. Scale bars are 10 μm in **A"** and 8 μm in both **C"** and **D"**. Biological replicates are N = 6 for 5-HT1A::GFP (**A-B**), N = 15 for L2>5-HT2B::sfGFP (**C-C"**), and N = 10 for L2>mCD8::GFP (**D-D"**).

were "presynaptic" to L2, T1 or L1 (S8B–S8E Fig). These data suggest that serotonergic signaling to L2, T1 (and perhaps other columnar neurons), is more likely to be mediated by volume transmission rather than true synaptic transmission, consistent with the use of volume transmission by most aminergic synapses in mammalian systems [95–98].

Serotonin increases calcium levels in L2 and L1 neurons

The data presented here and by others [70,71] strongly suggest that L2 and other cells in the visual system express serotonin receptors but do not address their function. To address the potential effects of serotonin on L2 neurons, we bath applied serotonin to the optic lobe and used live imaging to monitor cellular activity. The concentration of serotonin (100 μM) was within the range used in other *Drosophila* studies [89,99,100]. The data for receptor expression in L2 was strongest for 5-HT2B receptors, which couple with the $G_{q/11}$ protein alpha subunit to increase intracellular calcium *in vitro* [76,101]. We therefore used the genetically encoded calcium indicator GCaMP6f [102] to follow changes in L2 activity that we hypothesized could be induced by serotonin. We again employed the L2-split-GAL4 driver used for transcriptional analysis (Fig 2) to specifically express GCaMP6f in L2 neurons (Fig 4A). Since we observed enrichment of 5-HT2B::sfGFP in L2 terminals in M2, we focused our recordings of calcium signaling on these sites. For each experiment, we first recorded a baseline while perfusing the tissue with saline; the perfusion solution was then switched to either saline containing 100 μM serotonin or saline alone. Throughout the experiment, flies were exposed to a constant low-level luminance to control for visual input and tetrodotoxin (TTX) was included in the perfusion solution to reduce inputs to L2 neurons. In *Drosophila*, TTX inhibits the only known sodium channel $DmNa_V$ (formerly *para*) and represents a standard method to reduce neuronal inputs [99,103,104].

We consistently observed a large increase in GCaMP6f fluorescence in L2 terminals following serotonin application (Fig 4B and S9A Fig). This increase continued throughout the time course of the recordings, peaking at 1.73 ΔF/F ± 0.77 SEM (compared to saline control -0.03 ΔF/F ± 0.05 SEM at the same timepoint; p = 0.0095 by two-tailed Wilcoxon rank sum test). Thus, serotonin leads to an accumulation of cytosolic calcium in L2 cells, consistent with the predicted outcome of activating $G_{q/11}$-coupled 5-HT2B receptors [76,101].
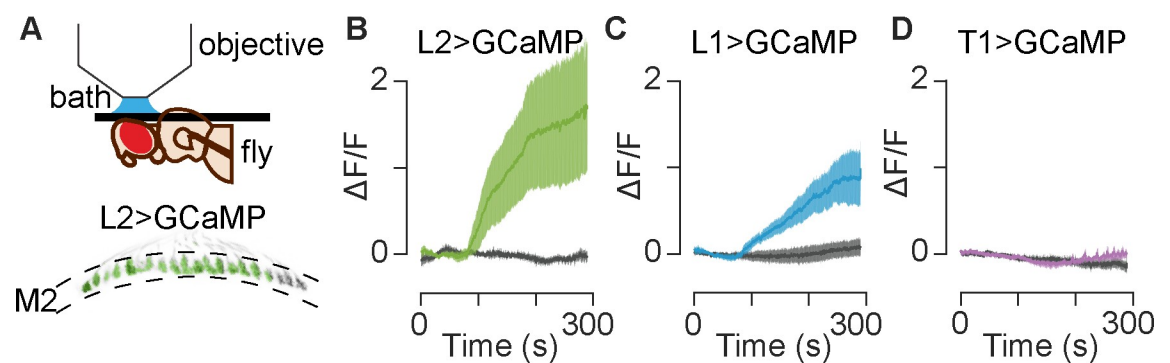
Fig 4. Bath application of serotonin leads to increased calcium in L2 and L1 neurons, but not T1 neurons. (**A**) The experimental setup is shown in the top of panel A, along with a sample image of L2 terminals (bottom of panel A, gray) as imaged in the medulla. The ROIs are overlaid in green. (**B-D**) GCaMP6f was paired with L2, L1 and T1 split-GAL4 drivers to monitor responses to 100 μM serotonin (colored traces) or saline controls (gray traces). The perfusion change occurred approximately 105 s into the recording, which corresponds to 45 s in (B-D) because the first 60 s are not shown. (**B**) In L2 terminals, serotonin application led to a significant increase in GCaMP6f signal indicating increased calcium levels as compared to saline controls (p = 00095). (**C**) L1 terminals showed a similar increase in calcium following a switch to serotonin (p = 0.02). (**D**) T1 cells expressing GCaMP6f showed no significant change in calcium following serotonin application (p>0.05). For (B-D) N = 4–8 individual flies; the dark trace is an average of all traces and the shaded region is 1 SEM; saline vs. serotonin comparisons are two-tailed Wilcoxon rank sum tests.

Since we did not detect serotonin receptors in L1 neurons, we did not expect serotonin to measurably change intracellular calcium levels in these cells. However, with GCaMP6f expressed in L1 cells using a cell-specific driver, we regularly observed a robust increase in fluorescence following serotonin exposure (Fig 4C and S9B Fig). Although the increase in GCaMP6f signal did not reach the same response amplitude as observed in L2 neurons, the time course was similar: the signal persisted throughout the recording and peaked at 0.98 ΔF/F ± 0.34 SEM (compared to saline control at 0.07 ΔF/F ± 0.09 SEM; p = 0.02 by two-tailed Wilcoxon rank sum test). A direct action of serotonin on L1 is unlikely since neither we (S7C Fig) nor others [70] detect endogenous serotonin receptors in L1 neurons. Possible mechanisms include inputs from either columnar or non-columnar neurons intrinsic to the visual system, more distal projections from the central brain, glial interactions or perhaps electrical coupling between L1 and L2 [28]. However, TTX was included in the perfusion solution in these experiments to reduce neuronal inputs to L1 including those mediated by action potentials and any graded potentials dependent on the *Drosophila* sodium channel $DmNa_V$ (formerly *para*) [103,104].

We next examined whether serotonin could affect the activity of T1 cells. Both 5-HT1A and 5-HT1B receptors, expressed in T1 neurons, are expected to couple with G_i proteins and negatively regulate adenylyl cyclase [74,101]. Due to the generally inhibitory function of these receptors, we hypothesized that serotonin would dampen activity in T1 neurons, possibly manifested as a decrease in cytosolic calcium or membrane potential [105]. Using the T1 split-GAL4 driver [90] to express either GCaMP6f or the voltage sensor Arclight [106], we did not observe a significant change in fluorescence during perfusion with serotonin (Fig 4D, S9C and S9D Fig) p>0.1). Thus, further experiments will be needed to determine the effects of serotonin on T1 neurons. These negative data are nonetheless important for the current study, since the absence of a GCaMP6f response in T1 neurons indicates that the responses observed in L1 and L2 are not artifacts or a generalized phenomenon common to all cells in the lamina.

Serotonin in visual processing

To explore the possibility that serotonergic neuromodulation plays a role in visual processing, we tested whether exogenous serotonin would alter visually induced calcium transients in L2 neurons. We used GCaMP6f to record and compare calcium transients in flies receiving saline or serotonin perfusion. Previous studies found that L2 neurons depolarize in response to dark flashes and hyperpolarize in response to light flashes [31,107]. Similarly, calcium-indicator recordings showed that intracellular calcium increased in the dark and decreased in the light [30,108]. Brief light or dark flashes induce bi-phasic calcium transients [31] that enable analysis of calcium kinetics. For this reason, we used brief dark or light flashes to test whether serotonin might alter the magnitude or kinetics of visually induced calcium transients in L2 terminals.

Flies were suspended over an LED arena (see Fig 4A) and either a light or dark flash of the entire LED screen (100 ms) was presented at 5-s intervals. Between each flash, the screen showed an intermediate brightness level, indicated as grey in Fig 5A. One-minute "epochs" consisting of 12 flashes of randomly shuffled polarity were presented six times for each trial (Fig 5A). The first 60-s epoch was recorded in saline alone, followed by a switch to either saline with 100 μM serotonin or saline alone during epoch 2 (Fig 5A). Unlike the experiments shown in Fig 4, we did not include TTX in these experiments so that we could measure L2 responses without dampening neuronal activity in response to visual stimuli.

Dark flashes induced a large increase in calcium that returned to basal levels within ~1 second as previously described [30,31,108] (Fig 5B). The amplitude of the dark flash-induced
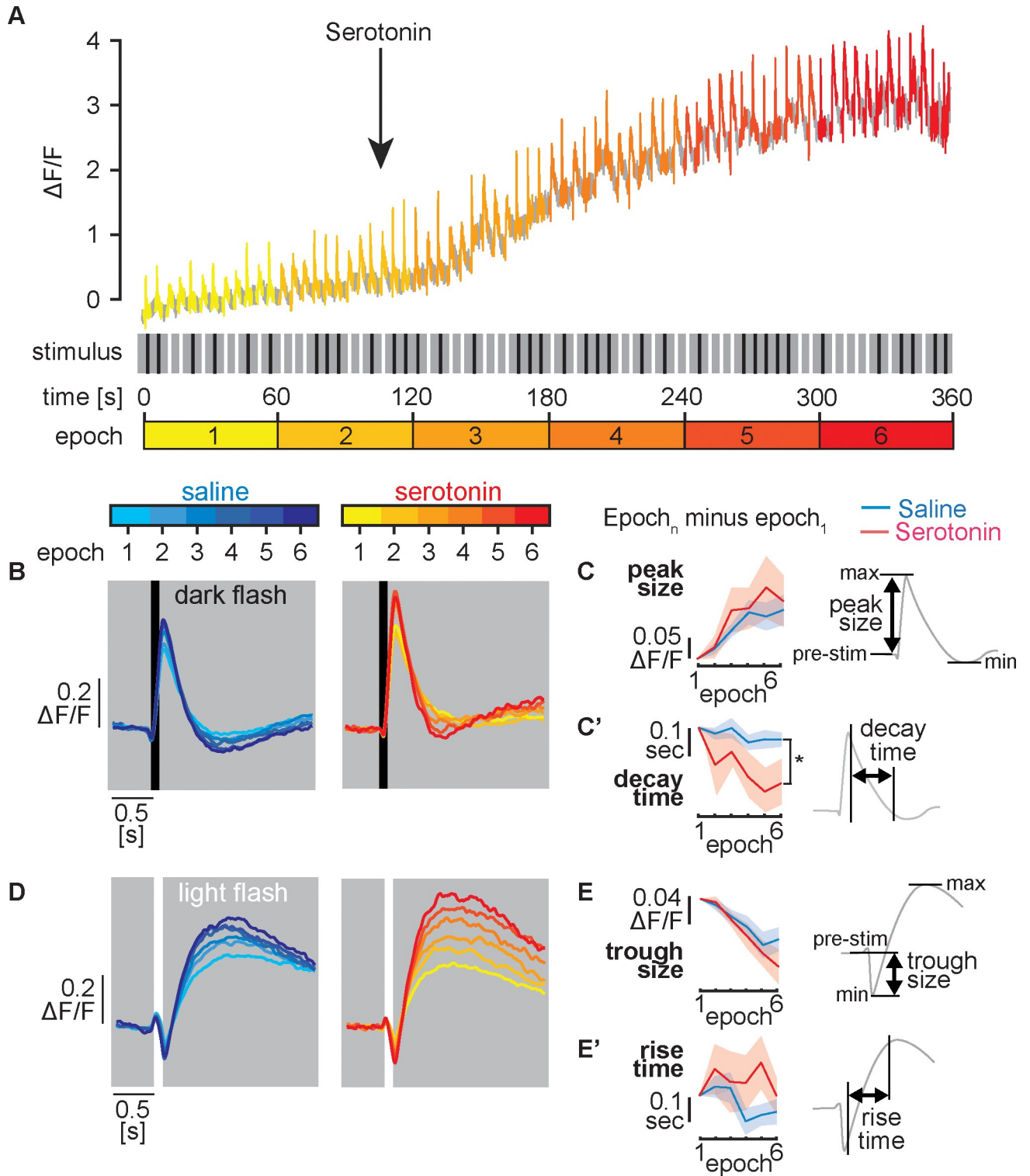
Fig 5. Serotonin modulates L2 neuron visually induced calcium transient kinetics. Visually induced calcium transients were recorded in flies expressing L2-split-GAL4>GCaMP6f. For all experiments, a baseline recording in saline (~105 s) was followed by perfusion with either serotonin or saline. (**A**) A sample recording is shown in the upper panel. Light or dark stimuli (A, middle panel, white and black vertical bars respectively) were flashed at random every 5 s for 6 min. To visualize changes in the response to light and dark flashes in L2, data from each 60 s epoch was binned (see epochs 1–6 in A, lower panel). (**B**) Response to dark flashes. Color coded traces representing each 60 s epoch are shown for flies receiving saline (left panel, cyan to blue) or serotonin perfusion (right panel, yellow to red). In both groups, L2 terminals responded to a dark flash with a strong increase in GCaMP6f

fluorescence. (**C-C'**) Analysis of dark flash response from panel B. For plotting each variable shown in C, the average value for the epoch 1 baseline was subtracted (Epoch$_n$-epoch$_1$). Epoch 1 is therefore always set to 0 in panel C-C". (**C**) The change in the calcium transient peak size (the difference between pre-stimulus $\Delta F/F$ and maximum $\Delta F/F$) relative to epoch 1. (**C'**) Change in time (s) from 90% to 10% of the peak-to-peak difference in $\Delta F/F$ (post stimulus max to min), relative to epoch 1. (**D**) Response to light flashes. When a light flash was presented in control experiments, L2 cells responded with a decrease in GCaMP signal followed by a large sustained increase in the GCaMP6 signal. Color coded traces representing each 60 s epoch for saline (left panel, cyan to blue) and serotonin (right panel, yellow to red) are shown. (**E-E'**) Analysis of light flash response from panel D. The average value for the epoch 1 baseline was subtracted as in panel C-C'. (**E**) Change in the calcium trough size (the difference between pre-stimulus $\Delta F/F$ and the subsequent minimum $\Delta F/F$) relative to epoch 1. (**E'**) Change in the time (s) from 10% to 90% of the peak-to-peak difference relative to epoch 1. Recordings in B-E represent, N = 14 and N = 20 individual flies perfused with serotonin or saline respectively. Shaded areas show mean +/- SEM. Comparisons are two-way repeated measures ANOVA with the bracket in 5C' indicating a significant effect of genotype (p≤0.05*).

calcium transients increased over the time course of the experiment for animals receiving either serotonin or saline (Fig 5B). To compare differences between the serotonin and saline control groups and the potential effects of serotonin over the time course of the experiment, we quantified calcium transient peak size (Fig 5C), the time required for decay from 90% to 10% of the peak-to-peak difference (post stimulus maximum minus post stimulus minimum) in $\Delta F/F$ (Fig 5C'), the exponential time constant of the decay (S10B Fig) and the size of the secondary response (S10A Fig). To facilitate the direct comparison of results obtained during perfusion with saline alone versus saline followed by serotonin, we first calculated the average for each variable prior to serotonin exposure measured during epoch 1. We then subtracted the epoch 1 baseline from each subsequent epoch and set the value of epoch 1 in each plot to 0 (indicated as Epoch$_n$-epoch$_1$ in Fig 5C and 5C').

We did not detect a difference between the serotonin and saline groups for changes in peak size (Fig 5C), the exponential time constant of the decay (S10B Fig) or the size of the secondary calcium response (S10A Fig). By contrast, we detected a modest, but statistically significant interaction between time and genotype (p = 0.04 by repeated measures two-way ANOVA) for the decrease in the decay time (Fig 5C').

Light flashes induced a transient decrease in GCaMP6f fluorescence, followed by a secondary calcium increase (Fig 5D) as previously reported [31]. To analyze calcium transients induced by light flashes, we quantified the trough size, defined as the magnitude of the initial calcium decrease relative to the pre-stimulus baseline (Fig 5E), the rise time, defined as the time from 10% to 90% of the peak-to-peak difference in $\Delta F/F$ (Fig 5E'), the exponential time constant of the rise time (S10D Fig) and the magnitude of the secondary response (S10C Fig). Epoch 1 baseline values obtained for the response to light flashes were again subtracted from each epoch to set the initial value of each variable to 0 for epoch 1 in Fig 5E and 5E'. We did not observe any significant differences between saline and serotonin groups when calculating the trough size (Fig 5E), rise time (Fig 5E'), the exponential time constant (S10D Fig) or the magnitude of the secondary response (S10C Fig).

In sum, serotonin drove a robust increase in intracellular calcium levels of L2 neurons in wildtype flies, regardless of the presence (Fig 4) or absence (Fig 5) of TTX. We also detected a modest, but statistically significant effect of serotonin on the decay time of the initial response to a dark flash, but not other metrics, and did not detect any effect of serotonin on the response of L2 to a light flash.

5-HT2B mediates the effects of serotonin on L2

Since 5-HT2B is expressed in L2 neurons and is predicted to use calcium as a second messenger, we hypothesized that it would mediate the GCaMP6 response of L2 neurons to serotonin. In flies expressing wild type 5-HT2B we observed a robust serotonin-mediated increase in basal intracellular calcium (Fig 4B and Fig 6A). We next examined whether loss of 5-HT2B would reduce the gradual increase in basal calcium we observed in flies exposed to serotonin

(Fig 6B). As a negative control for experiments using the 5-HT2B homozygous mutants (-/-) we used heterozygous siblings (+/-) in which one wild type allele of 5-HT2B was present (Fig 6B). Similar to 5-HT2B +/+ flies (Fig 6A), 5-HT2B heterozygous controls perfused with serotonin showed a gradual increase in basal calcium levels over the six-minute time course of the experiment (Fig 6B). In contrast, in the 5-HT2B -/- mutant, the basal calcium signal was nearly flat over the time course of the experiment (p = 0.0024 by two-tailed Wilcoxon rank sum test). Although we cannot rule out indirect effects from 5-HT2B expression in other cell types, the simplest explanation for the observed results is that activation of 5-HT2B in L2 neurons generates a gradual increase in cytosolic calcium.

We next examined whether loss of 5-HT2B would alter the calcium transients in L2 neuron terminals following light or dark flashes. As a negative control, we again used heterozygous siblings (5-HT2B +/-). During epoch 1, the period before serotonin perfusion, the magnitude of both the dark-induced calcium increase and light-induced decrease was larger in 5-HT2B +/- compared to 5-HT2B -/- flies (compare Fig 6C and Fig 6E). Further experiments will be needed to determine the origin of this effect and whether it could distort the cells' response to serotonin.

To compare how the loss of 5-HT2B might affect the response to serotonin perfusion, we graphed averages for each epoch after subtraction of the average for epoch-1—the same approach we used in Fig 5C and 5E. As we observed in 5-HT2B +/+ flies (see Fig 5C'), perfusion of both 5-HT2B +/- heterozygous controls and 5-HT2B -/- flies with serotonin led to a gradual reduction in the time required for L2 terminals to reach a minimum after responding to a dark flash (Fig 6D'). The effects on peak size (Fig 6D) were not statistically significant (p = 0.08) between the 5-HT2B -/- mutant and heterozygous controls despite the apparent divergence of the curves. The decay time (Fig 6D and 6D'), size of the secondary response (S11A Fig) and the exponential decay constants (S11B Fig) were also similar, although the final time point for the exponential decay showed a modest difference between the 5-HT2B -/- mutant and heterozygous controls (S11B Fig).

In response to light flashes, the 5-HT2B +/- heterozygote preparations showed a progressive increase in the magnitude of the trough size (Fig 6F); this progression was absent in 5-HT2B -/- mutants. The interaction between the time course and genotype was highly significant (p≤0.0001), the effect of genotype alone was also significant (p = 0.0026) (Fig 6F), and in post hoc tests multiple time points differed between heterozygotes versus homozygotes. Conversely, the rise time (Fig 6F'), the size of the secondary response (S11C Fig) and the exponential time constant (S11D Fig) did not significantly differ between the mutant versus control (Fig 6F'). In sum, the differences between 5HT2B +/- and 5-HT2B -/- in at least one measure of their response to a light flash suggest that 5-HT2B may regulate the effects of serotonin on the response of L2 neurons to some visual stimuli.

Discussion

To develop the fly visual system as a molecular-genetic model to study serotonergic neuromodulation we have confirmed the expression of the five *Drosophila* serotonin receptors in a subset of experimentally tractable cells in the lamina and used live imaging to determine their physiological effects. Our data are generally consistent with two previous transcriptomic studies by Davis et al. [70] and Konstantinides et al. [71] and indicate that L2 cells express 5-HT2B, T1 cells express both 5-HT1A and 5-HT1B, and L1 does not express detectable levels of any serotonin receptors. Our data are also consistent with the expression of 5-HT1A in C2 cells and 5-HT7 in L5 cells. In S2 Fig we directly compare our current findings with those of Davis et al. [70] and Konstantinides et al. [71]. Although our RT-qPCR data support the possibility
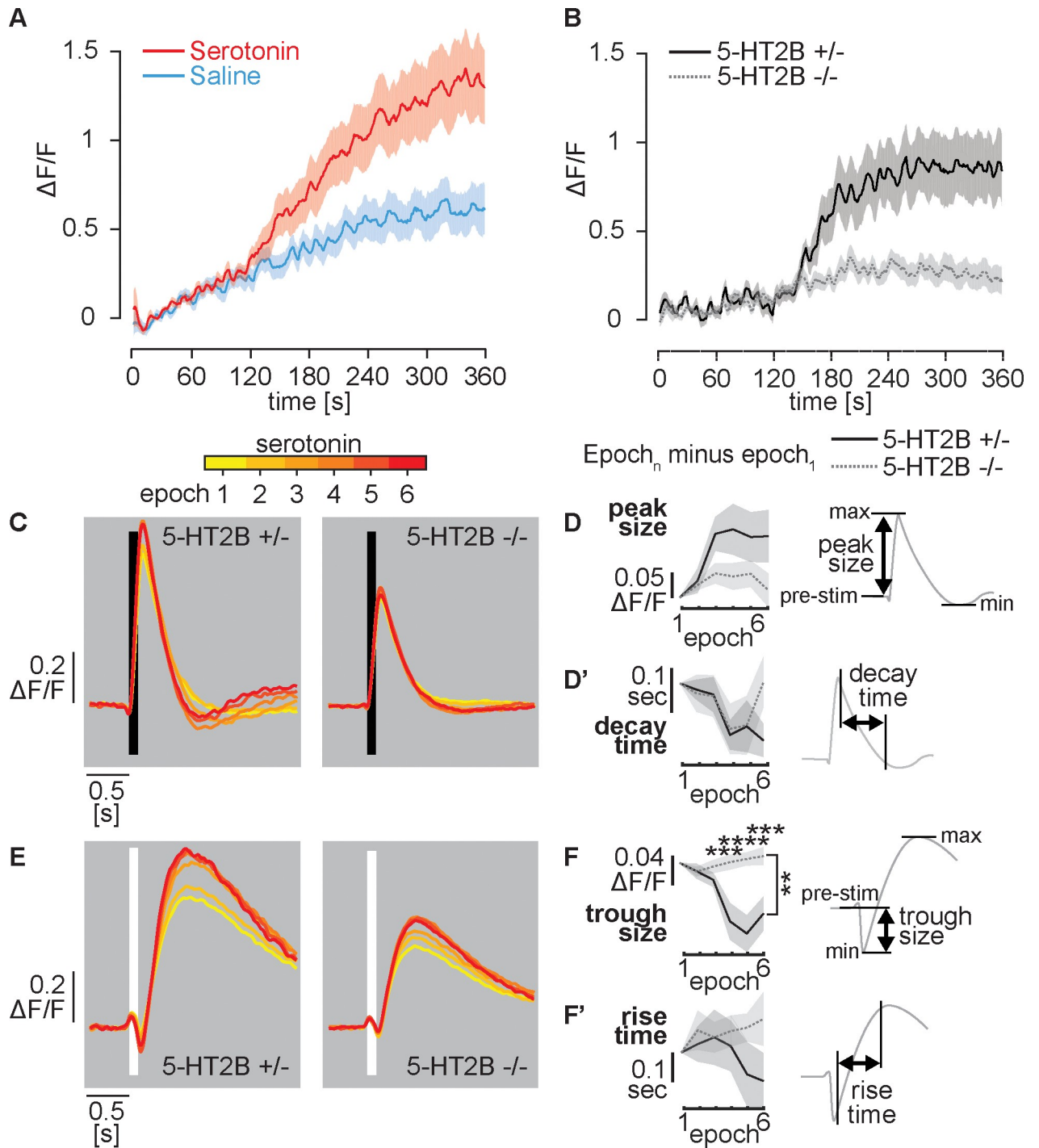
Fig 6. 5-HT2B mediates the L2 neuron response to serotonin. Perfusion with serotonin or saline alone was initiated ~105 s after baseline recording in saline as in Fig 5. (**A**) L2>GCaMP6f response of wild 5-HT2B +/+ flies to serotonin versus saline perfusion in the absence of TTX. (**B**) L2>GCaMP6f response of homozygous (5-HT2B -/-) and heterozygous (5-HT2B +/-) flies to serotonin perfusion. (**C-F**) Calcium transients following brief light or dark flashes in homozygous (5-HT2B -/-) and heterozygous (5-HT2B +/-) flies. Metrics and analysis are identical to those described in Fig 5. For (A), N = 14 serotonin and N = 20 saline exposed flies were tested. For (B-F), N = 13 5-HT2B +/- and N = 15 5-HT2B -/- flies, all receiving serotonin, were tested. Shaded areas show mean +/- SEM. Comparisons in (D, F) are two-way repeated measures ANOVA (brackets show interactions between time and genotype) and Sidak's multiple comparisons tests for indicated time points, $p \leq 0.01^{**}$, $p \leq 0.001^{***}$, $p \leq 0.0001^{****}$.

that L2 neurons might also express 5-HT7, neither we nor others detect an enrichment of 5-HT7 using RNA-Seq [70].

The MCFO stochastic labeling approach used in Fig 1 is based on the assumption that MiMIC-driven GAL4 expression is transcriptionally linked to gene expression and so may be more likely to occur in cells where the gene is more highly expressed. For this reason, the MiMIC-based screening approach could be biased toward more highly expressed genes and may provide a less comprehensive picture of expression compared to sequencing approaches. Although Konstantinides et al. [71] report expression of 5-HT1A and two additional receptors (5-HT1B and 5-HT7) in C2 neurons, they report expression levels for 5-HT1A approximately 30 times higher than either 5-HT1B or 5-HT7. We did not detect 5-HT1B or 5-HT7 in centrifugal C2/C3 cells, and this may result from lower levels of expression in these cell types. Unlike Davis et al. [70] we did not detect expression of serotonin receptors in either photoreceptor cells or in lamina monopolar neuron L3 using MiMIC-T2A-GAL4>UAS-MCFO. In addition to low levels of expression, the inconsistencies between data sets could be due to biological variability in levels of gene expression or infidelity in the MiMIC-based approach, which may not perfectly reflect endogenous expression. Differences between our genomic data and that of others may also reflect variation in the methods used to isolate target cell populations, extract RNA, or create DNA libraries for sequencing. For example, TAPIN-seq involves successive rounds of immunoprecipitation, which can be affected by non-specific antibody binding to ambient RNA or off-target proteins. By contrast, our use of FACS can lead to contamination by other cell types due to incomplete dissociation of GFP-tagged cells or due to non-specific labeling by the driver lines.

Consistent with the predicted coupling of 5-HT2B to G_q, we found that L2 neurons respond to serotonin with a robust increase in basal calcium measured by GCaMP6f fluorescence (Fig 4B, Fig 6A, S9A Fig) and this effect was dramatically reduced in 5-HT2B -/- flies (Fig 6B). The simplest explanation for these effects is that 5-HT2B expressed in L2 regulates the increase in basal calcium. Specific knockdown of 5-HT2B in L2 neurons will be required to address this important issue. Since RNAi lines can be ineffective or yield off-target effects, additional genetic tools may be useful to perform cell type specific knock down or knock out experiments [109]. Additional experiments will also be needed to assess the potential developmental effects of the 5-HT2B mutant, and in particular how loss of 5-HT2B may have altered the baseline response of L2 to visual stimuli in the absence of exogenous serotonin. Finally, we cannot completely rule out the possibility that 5-HT7 could contribute to the regulation of at least some L2 cells (see S7B Fig). These limitations aside, our data indicate that 5-HT2B induces robust increases in basal levels of intracellular calcium in L2 neurons.

In L1 neurons, which do not express serotonin receptors, we unexpectedly observed a large basal calcium response to serotonin similar to that of L2 neurons (Fig 4C). The most likely explanation would seem to be activation of L1 neurons by input from cells that express serotonin receptors either in the optic lobes or perhaps the central brain. GABAergic C2 neurons [110] may express 5-HT1A (S2 Fig, S3D and S3E Fig) and are known to synapse onto L1 in M1 [36]. Likewise, L5 neurons may express the 5-HT7 receptor (Fig 1E, S2 Fig) and reciprocally synapse with L1 neurons in M1 and M5 [36]. L1 recordings were performed in the presence of TTX, which blocks the *Drosophila* sodium channel $DmNa_V$ formerly (*para*) [111, 112] and represents a standard method to reduce neuronal inputs [103,104]. While TTX is expected to inhibit most if not all action-potentials, graded potentials, which are common in the fly [113–115] could activate L1 if these inputs were not influenced by inhibition of $DmNa_V$. Alternatively, indirect serotonergic regulation of L1 neurons might occur through gap junctions previously shown to couple L1 and L2 neurons [28]. In addition, we and others [70,84] detect serotonin receptor expression in glia (S4 Fig), and it is possible that activation of the serotonin

receptors in lamina glia could indirectly influence L1, perhaps via regulation of extracellular ion concentrations [116,117].

The only prior report of an acute physiological response to serotonin in the *Drosophila* visual system described the modulation of potassium channels in photoreceptors [44]. However, the ex vivo preparations used for these experiments may have included other cells or cell fragments, and unlike a previous transcriptomic study [70], we did not detect serotonin receptor expression in photoreceptors. We speculate that, similar to L1, serotonin may indirectly regulate photoreceptors via inputs from other neurons such as L2 or lamina glia [27,44,118].

Serotonin is implicated in circadian rhythms [55,56] and both L1 and L2 terminals exhibit rhythmic daily size changes in the medulla that are mediated by both serotonin [59] and glia [119]. Tissue levels of serotonin levels also decrease in constant darkness [56], and T1 neurons have been shown to be involved in circadian entrainment via expression of *timeless2* [120]. It is tempting to speculate that the acute increase in basal calcium we observed in response to exogenous serotonin (Fig 4B and 4C) could be relevant to circadian changes in the function of L1 and L2. In future experiments, it will be interesting to examine more chronic effects of serotonin on the physiology of L2 and whether 5-HT2B is also involved in these phenomena.

In T1 neurons, we were unable to detect any acute changes in basal calcium or voltage in response to serotonin application (Fig 4D and S9C and S9D Fig) and other probes (e.g., for cAMP) may be necessary to detect the acute response of T1 to serotonin. However, it is also possible that activation of 5-HT1 receptors does not induce any acute physiological response, and that more chronic indices will be necessary to detect the potential effects of serotonin on T1 neurons. For now, the absence of a GCaMP6f response in T1 neurons serves as an important negative control and demonstrates the specificity of the responses observed in L1 and L2.

Based on the localization of the tagged 5-HT2B receptor, we suggest that serotonin acts on L2 terminals in the medulla neuropil. While we do not know the physiological effects of serotonin on T1, we find that a tagged version of 5-HT1A expressed via the 5-HT1A locus in T1 and other cells localized to a similar site in the medulla neuropil (Fig 3). The localization of 5-HT1A and 5-HT2B to nerve terminals suggests that they could regulate presynaptic neurotransmitter release. If so, future experiments may reveal that serotonergic inputs to L2 regulate the physiological response to visual stimuli in neurons that are post-synaptic to L2.

Coordinated regulation of multiple terminals by a single serotoninergic neuron may be facilitated by the extrasynaptic release of serotonin through volume transmission, the primary mode of signaling in most aminergic circuits within the mammalian CNS [48,121–124]. Serotonergic release sites appear to lack synaptic partners in the lamina of the blowfly *Calliphora* [125] and our data using sybGRASP to test whether serotonergic neurons synapse onto L2, T1, and L1 was negative (S8 Fig). Recent advancements such as the full adult fly brain EM dataset [126] combined with predictive neurotransmitter mapping [127] will be important resources to determine the precise relationship between serotonergic boutons and the nerve terminals within the medulla neuropil. Further studies will also be needed to define the function of putative serotonin autoreceptors which we and others detect in serotonergic neurons (S5 Fig, S6 Fig and Fig 3B) [56,89]. While the importance of serotonergic autoreceptors in mammalian circuits is well established [128–130], their function in the fly is not well described.

We observed serotonin-mediated increases in basal calcium in L2 neuron terminals, which correlated with more subtle modulation of visually induced calcium transients following serotonin application (Figs 5 and 6). It is possible that the modest changes in calcium transient dynamics represent a role for serotonin in potentiating the response of L2-dependent visual processing pathways [31]. However, it is difficult to rule out the possibility that the non-linear dynamics of GCaMP6f could influence and perhaps account for the differences we observe between groups. Further experiments using other reporters may be useful to confirm our

observations. If validated, our data may suggest a molecular-mechanism for previous observations made in larger insects including serotonin-induced changes field potentials in blowfly representing the output of lamina monopolar cells [53] and honeybee motion detection in the lobula [45].

We observed differences in the visual responses of 5-HT2B +/- and 5-HT2B -/- even before serotonin perfusion. This might result from the activation of 5-HT2B by endogenously released serotonin or developmental defects caused by loss of 5-HT2B. It is possible that such developmental defects could broadly disrupt the physiology of L2 neurons and thereby confound our interpretation of the cell's response to exogenous serotonin. Future experiments to inducibly block the activity of 5-HT2B and/or endogenous serotonin in the adult but allow wild type activity during development will be needed to address this possibility. While the serotonin concentration used in our experiments is comparable to other studies in *Drosophila* [89,99,100] it is difficult to mimic the physiological environment using bath applied neurotransmitters. Future experiments using optogenetic stimulation will be needed to address this issue.

The relationship between repeated visual stimuli and basal calcium levels will also require further investigation. During the initial period before exogenous serotonin perfusion, the basal calcium levels of flies exposed to repeated visual stimuli (Fig 6A) increased while those shown a constant, medium luminance screen (Fig 4B) did not appreciably change. We speculate that the repeated visual stimuli may have induced the modest increase in basal calcium observed in Fig 6A as part of an adaptive response. It is possible that activation of 5-HT2B by endogenously released serotonin could be responsible for this effect.

The increase in basal calcium following serotonin perfusion could potentially affect previously identified properties of L2. These include surround inhibition mediated by the GABA-A channel Rdl [131]. If rising basal calcium is accompanied by a tonic membrane depolarization further from the Cl^- reversal potential, the driving force on GABA-A mediated Cl^- current would be expected to increase. If so, serotonin might change the spatial structure of surround inhibition as well as tip the balance between ON and OFF response components to favor ON stimulation. Cell-specific manipulation of *Rdl* and/or 5-HT2B might be used to test this hypothesis [109,132].

Studies in mammals have already begun to dissect the contributions of serotonergic tuning in multiple cells within individual circuits including the visual system [6,18,23,133,134] but the way in which this information is integrated remains poorly understood. The interactions between receptors expressed on L2 and other neurons in the fly visual system provide a new framework to dissect the mechanism by which multiplexed serotonergic inputs combine to regulate circuit function.

Conclusion

We have demonstrated that a subset of cells in the lamina express serotonin receptors and respond to exogenous serotonin with a robust increase in basal calcium and a more modest change in their physiological response to visual stimuli. Further experiments will be needed to determine how these changes affect circuit output and processes that occur over longer time scales.

Methods

Fly husbandry and genetic lines

Flies were maintained on a standard cornmeal and molasses-based agar media with a 12:12 hour light/dark cycle at room temperature (22–25˚C). All fly strains used in this study are

listed in S3 Table. Serotonin receptor MiMIC-T2A-GAL4 lines described in [77] were a gift from Herman Dierick (Baylor College of Medicine), and include 5-HT1A-T2A-GAL4^{MI01468}, 5-HT1A-T2A-GAL4^{MI01140}, 5-HT1A-T2A-GAL4^{MI04464}, 5-HT1B-T2A-GAL4^{MI05213}, 5-HT2A-T2A-GAL4^{MI0459}, 5-HT2A-GAL4^{MI03299}, 5-HT2B-T2A-GAL4^{MI06500}, 5-HT2B-T2A-GAL4^{MI5208}, 5-HT2B-GAL4^{MI7403}, and 5-HT7-GAL4^{MI00215}. L1- and T1-split-GAL4 lines [90], as well as unpublished LexA lines for L1 and T1, were generously provided by Aljoscha Nern and Gerry Rubin (HHMI/Janelia Research Campus). S.L. Zipursky (UCLA) generously provided L2-split-GAL4 and L2-LexA (RRID:BDSC_52510). Yi Rao (Peking University) generously shared 5-HT2B-KO-GAL4 SII (5-HT2B mutant) [93], 5-HT1A::sfGFP [92], and UAS-5-HT2B::sfGFP [93].

SerT-GAL4 (RRID:BDSC_38764), GAD1 Trojan LexA (RRID:BDSC_60324) and ChAT Trojan LexA (RRID:BDSC_60319) were obtained from Bloomington *Drosophila* Stock Center (BDSC) at Indiana University (Bloomington, IN, USA). Additional reporters from BDSC include: UAS-mCD8::GFP (RRID:BDSC_5137), UAS-MCFO-1 (RRID:BDSC_64085), UAS-GCaMP6f (RRID:BDSC_42747), UAS-ArcLight (RRID:BDSC_51056), UAS-mCD8::RFP, LexAop-mCD8::GFP (RRID:BDSC_32229), and UAS-nSyb::GFP1-10, LexAop-CD4:GFP11 (RRID:BDSC_64314; provided through S.L. Zipursky (UCLA)).

Immunofluorescent labeling and imaging

Flies were dissected 5–10 days after eclosion, and equal numbers of males and females were used for all experiments unless otherwise noted. Brains were dissected in ice-cold PBS (Alfa Aesar, Cat#J62036, Tewksbury, MA), then fixed in 4% paraformaldehyde (FisherScientific, Cat#50-980-493, Waltham, MA) in PBS with 0.3% Triton X-100 (Millipore Sigma, Cat#X100, Burlington, MA) (PBST) for one hour at room temperature. After fixation, brains were washed three times with PBST for 10 minutes, then blocked for 30 minutes in PBST containing 0.5% normal goat serum (NGS) (Cayman Chemical, Cat#10006577, Ann Arbor, MA). Antibodies were diluted in 0.5% NGS/PBST. Primary antibodies were incubated with the tissue overnight at 4°C. The next day, the brains were washed three times with PBST for 10 minutes, then incubated with secondary antibodies for 2 hours in the dark at room temperature. Brains were washed three times with PBST for 10 minutes before mounting.

For frontal mounting, brains were washed with 60% and 80% glycerol (Millipore Sigma, Cat#G5516) and mounted in Fluoromount-G (SouthernBiotech, Cat#0100–01, Birmingham, AL). For dorsal-ventral mounting, brains were fixed in 2% PFA/PBST overnight. The next day, brains were washed three times with PBST. Brains were dehydrated with a series of 10 min ethanol baths of increasing concentrations (30%, 50%, 75%, 95%, 100%, 100%, and 100%). Brains were then transferred to 100% xylene before mounting in DPX (FisherScientific, Cat#50-980-370).

Serotonin immunolabeling was performed with 1:25 rat anti-serotonin (Millipore Sigma, Cat#MAB352, RRID:AB_11213564), 1:1000 rabbit anti-serotonin (ImmunoStar, Cat#20080, Hudson, WI, RRID:AB_572263) or 1:1000 goat anti-serotonin (ImmunoStar, Cat#20079, RRID:AB_572262). Where noted, GFP was labeled with 1:250 mouse anti-GFP (Sigma-Aldrich, Cat#G6539, RRID:AB_259941; or, ThermoFisher, Waltham, MA, Cat#A-11120, RRID:AB_221568). Secondary antibodies were used at 1:400 and include: Donkey anti-mouse Alexa Fluor 488, Donkey anti-Rabbit Alexa Fluor 594 or Alexa Fluor Donkey anti-rat 647 (Jackson ImmunoResearch Laboratories, Westgrove, PA, Cat#715-545-151, # 711-585-152, # 712-605-153) or Alexa Fluor 555 (Life Technologies, ThermoFisher, Cat#A-21428).

When serotonin receptor MiMIC-GAL4 lines were combined with ChAT or GAD1 MiMI-C-LexA (S3 Fig), brains were processed and imaged as described in Sizemore and Dacks 2016 [135]. MultiColor FlpOut (MCFO-1) sparse labeling was induced by heat activation at 37°C for

10–15 minutes at least 2 days prior to dissection as described [82]. Although MCFO can be used for lineage tracing [82], we induced MCFO in adult flies, when visual system neurons are post-mitotic, and MCFO labeling does not represent clonal events. Primary antibodies included 1:300 rabbit anti-HA (Cell Signaling Technology, Cat#3724, Danvers, MA, RRID:AB_1549585), 1:150 rat anti-FLAG (Novus, Littleton, CA, Cat#NBP1-06712, RRID:AB_1625982), and 1:400 mouse anti-V5::Dylight-550 (Bio-Rad, Hercules, CA, Cat#MCA1360D550GA, RRID:AB_2687 576). The rat anti-N-Cadherin (DN-Ex#8) and mouse anti-repo (8D12 concentrate) was obtained from the Developmental Studies Hybridoma Bank, created by the NICHD of the NIH and maintained at The University of Iowa, Department of Biology, Iowa City, IA 52242. Secondary antibodies used for MCFO are listed above. N-Synaptobrevin GFP Reconstitution Across Synaptic Partners (sybGRASP) flies [94] were dissected, fixed and immunolabeled as described above, without KCl induction. The tissue was labeled with mouse antiserum specific to reconstituted GFP (1:250; Sigma-Aldrich, Cat#G6539, RRID:AB_259941) [136] and either anti-serotonin (antibodies listed above).

Imaging was performed with a Zeiss LSM 880 Confocal with Airyscan (Zeiss, Oberkochen, Germany) using a 40x water or 63x oil immersion objective. Post-hoc processing of images was done with Fiji [137] or Adobe Photoshop (Adobe, San Jose, CA).

FACs and RNA extraction

L2 and L1 neurons were labeled using split-GAL4 drivers combined with UAS-mCD8::GFP (RRID:BDSC_5137). For RNA-Seq in Fig 2, N = 3 T1-LexA samples were tested. For RT-qPCR in S7 Fig, we included N = 3 T1-split-GAL4 samples and N = 3 T1-LexA samples. Brains were dissected on the day of eclosion and optic lobes were dissociated according to previously published methods [138]. The dissociated optic lobe cells were separated by fluorescence-activated cell sorting (FACS) into GFP-positive and GFP-negative isolates using a BD FACS Aria II high-speed cell sorter in collaboration with the UCLA Jonsson Comprehensive Cancer Center (JCCC) and Center for AIDS Research Flow Cytometry Core Facility (http://cyto.mednet.ucla.edu/home. html). For FACS, each experiment was performed with 18–40 brains, and yielded between 1,700–7,800 GFP$^+$ cells. RNA was extracted from isolated cells with ARCTURUS® PicoPure® RNA Isolation Kit (ThermoFisher, KIT0204) or RNeasy Plus Micro Kit (QIAGEN, 74034).

RT-qPCR

RNA extracted from FACS isolates was reverse transcribed using SuperScript III (Invitrogen, ThermoFisher, Cat#18080093). RT-qPCR was performed for receptor cDNA using validated primers (S4 Table) and SYBR Green Power PCR Mix (Applied Biosystems, ThermoFisher) on an iQ5 real-time qPCR detection system (Bio-Rad). Primers were designed using Primer-Blast (https://www.ncbi.nlm.nih.gov/tools/primer-blast/) or were from the DGRC FlyPrimerBank [139]; oligonucleotides were obtained from Integrated DNA Technologies (Coralville, Iowa). Primer pairs were validated to amplify a single product, verified by a single melting temperature and single band on an electrophoresis gel. The efficiency for each primer pair was between 85–115%. Comparisons between GFP$^+$ and GFP$^-$ samples were calculated as enrichment (i.e., fold change) using the comparative CT method [91]. A zero value was imputed for samples with no amplification (i.e., no CT value). Raw CT values are shown in S2 Table.

RNA-Seq

RNA-Seq was performed using a SMART-Seq protocol adapted from [138,140,141]. Libraries were constructed using the SMART-seq v4 Ultra Low-input RNA sequencing kit with Nextera XT (Takara Bio). Paired-end sequencing was conducted by the UCLA genomic core facility

(https://www.semel.ucla.edu/ungc/services). After demultiplexing, we obtained between 39–270 (average 105) million reads per sample. Quality control was performed on base qualities and nucleotide composition of sequences. Alignment to the *Drosophila melanogaster* genome (BDGP6) was performed using the STAR spliced read aligner [142] with default parameters. Additional QC was performed after the alignment to examine the following: level of mismatch rate, mapping rate to the whole genome, repeats, chromosomes, and key transcriptomic regions (exons, introns, UTRs, genes). Between 75–85% of the reads mapped uniquely to the fly genome. Total counts of read fragments aligned to candidate gene regions within the reference gene annotation were derived using HTSeq program and used as a basis for the quantification of gene expression. Only uniquely mapped reads were used for subsequent analyses. Following alignment and read quantification, we performed quality control using a variety of indices, including consistency of replicates and average gene coverage. For Fig 2, L2 samples were run in two separate sequencing runs and we did not perform corrections for any potential batch effects. Data is shown as Transcripts Per Million (TPMs). The RNA-Seq data (raw and processed files) are available on GEO at https://www.ncbi.nlm.nih.gov/geo/query/acc.cgi?acc=GSE154085.

Live cell imaging

Calcium imaging was performed as previously described [132,143,144]. Briefly, flies were anesthetized at 4°C and placed into a chemically etched metal shim within a larger custom-built fly holder. The fly holder was based on a previously described design [145]. The head capsule and the thorax were glued to the metal shim using UV-curable glue (www.esslinger.com). The legs, proboscis and antennae were immobilized using beeswax applied with a heated metal probe (Waxelectric-1, Renfert). The head capsule was immersed in insect saline (103 mM NaCl, 3 mM KCl, 1.5mM CaCl2, 4 mM MgCl2, 26 mM NaHCO3, 1 mM NaH2PO4, 10 mM trehalose, 10 mM glucose, 5 mM TES, 2 mM sucrose) [146]. A small window on the right rear head capsule was opened using sharp forceps (Dumont, #5SF). Muscles and fat covering the optic lobe were cleared before placing the fly under the 2-photon microscope (VIVO, 3i: Intelligent Imaging Innovations, Denver, CO). Neurons expressing GCaMP6f were imaged at 920-nm using a Ti:Sapphire Laser (Chameleon Vision, Coherent). Images were acquired at 10–20 frames/s for Fig 4 and 25–30 frames/s for Figs 5 and 6 live imaging. Only female flies were used for live imaging experiments.

A custom-built gravity perfusion system was used for bath application of either serotonin or saline control to the fly's exposed optic lobe for Fig 4. For Fig 4 and S9 Fig, the tissue was first perfused with insect saline containing 1µm tetrodotoxin citrate (TTX) (Alomone Labs, Jerusalem, Israel, Cat#T-550) for at least 5 minutes at 2 mL/min, prior to each recording. TTX remained present throughout the experiment. To examine the effects of serotonin on calcium levels, baseline GCaMP6f fluorescence was recorded for one minute before switching to the second input containing either 100 µM serotonin hydrochloride (Sigma Aldrich, Cat# H9523) or saline alone for an additional five minutes of recording. The concentration of serotonin used is comparable to recent physiological studies applying exogenous serotonin to the *Drosophila* brain [89,99,100]. Due to perfusion tubing length and dead volume, the perfusion switch took approximately 105 s to reach the tissue. Fig 4 does not show the first minute of the recording, so the solution switch occurs at approximately 45 s on the x axis. For more precise control of perfusion solutions, we used a programmable valve controller (VC-6, Warner Instruments, Hamden, CT) for Figs 5 and 6 visual experiments (see details below).

Visual stimulus experiments

Visual stimuli were shown using an arena composed of 48 eight by eight-pixel LED panels, at 470 nm (Adafruit, NY, NY). The panels were assembled into a curved display that extends

216˚ along the azimuth and ±35˚ in elevation. Each pixel subtended an angle of 2.2˚ on the retina at the equatorial axis. To prevent spurious excitation of the imaging photomultiplier tubes, three layers of blue filter (Rosco no. 59 Indigo) were placed over the LED display.

Each stimulus consisted of a brief increment (light flash) or decrement (dark flash) of the entire display for 100 ms, before returning to a mid-intensity brightness for 4.9 s. Images were acquired at 25–30 frames/s for Figs 5 and 6 visual stimulation experiments. Stimuli were presented in sets of six bright and six dark flashes randomly shuffled for each minute of the experiment. Responses were then pooled for each minute. During the first minute ("epoch 1" in Figs 5 and 6), and prior to imaging, the tissue was perfused with saline for a baseline recording. At the end of the first minute, a valve controller (VC-6, Warner Instruments, Hamden, CT) activated by a TTL signal switched the perfusion to either saline with 100 μM serotonin or saline alone; imaging then continued for an additional five minutes, for a total of one baseline set and five post-switch sets of stimuli. The perfusion switch took approximately 45 s to reach the tissue using the programmable valve system.

Analysis

The analysis code and the live-imaging data has been deposited at https://osf.io/39j4m/ (DOI: 10.17605/OSF.IO/39J4M). Calcium imaging data were analyzed with Matlab R2017a (Mathworks, Natick, MA). Post hoc, recordings were corrected for movement of the brain within the imaging plane using a custom algorithm [147]. Regions of interest (ROIs) were found semi-automatically for data in Figs 4–6: first, the median intensity of all pixels across all image frames was found; this value was used as a threshold and all pixels with mean intensity below the threshold, typically within the image background, were discarded. The 1-D time series of intensity for each remaining pixel was then extracted. K-means clustering was used to identify pixels with similar activity over the course of the experiment: three clusters were identified and the cluster with the highest number of pixels was retained. This reliably identified the pixels within active neurons in the imaging data and aided in identifying preparations with out-of-plane movement, which were discarded.

For basal calcium experiments (Fig 4), the remaining cluster was used as a single ROI and the mean intensity within the ROI was found for each image frame to produce a single time-series for the entire experiment. For visual response experiments (Figs 5 and 6), pixels within the remaining cluster were automatically divided into groups corresponding to individual L2 terminals using a watershed transform. The mean intensity within each ROI was found for each image frame to produce a single time-series for the entire experiment, and the time-series for all terminal ROIs within an individual animal were then averaged. For Fig 6, ROIs of L2 terminals were first identified automatically, as above, then manually selected individually according to layer position because the 5-HT2B GAL4 SII mutant line labeled other cells in addition to L2 neurons.

Approximately half of the bath application recordings showed oscillations in activity due to slow, periodic movement of the brain at around 0.04 Hz; we applied a second-order notch filter at this frequency with a bandwidth of 0.005 Hz to remove these oscillations. For the bath application experiments (Fig 4), we plotted $\Delta F/F$, defined as $(F_t - F_0)/F_0$, where F_t is the mean fluorescence in the ROI at the indicated time and F_0 is the mean value of F_t during 60 seconds of baseline activity at the beginning of the experiment and prior to the change in perfusion. For the visual stimulus experiments (Figs 5 and 6), we again plotted $\Delta F/F$, defined as $(F_t - F_0)/F_0$, where F_t is the mean fluorescence across all individual terminal ROIs at the indicated time and F_0 is the mean of 30 seconds of non-consecutive baseline activity between stimulus presentations during epoch 1 at the beginning of the experiment and prior to the change in perfusion

(Fig 5A). For the stimulus response plots (Figs 5B, 5D, 6C and 6E), we found the average $\Delta F/F$ time-series within each epoch for each fly after subtracting the average pre-stimulus baseline activity level (0.5 s preceding each flash stimulus) from each time-series, so that all responses started aligned at 0 $\Delta F/F$. For further analysis (Figs 5C, 5E, 6D and 6F), we calculated the changes in response amplitude across epochs, defined for the dark stimulus presentation as the difference between the pre-stimulus baseline and the maximum post-stimulus $\Delta F/F$ value. For each epoch$_n$, we subtracted the value of the responses during epoch 1 at the beginning of the experiment and prior to the change in perfusion (indicated in the Figs 5 and 6 as "Epoch$_n$ minus epoch$_1$"), in order to find the change in amplitude relative to epoch 1. We followed a similar procedure for the secondary calcium responses (S10-S11) the decay (or rise) time (Figs 5C', 5E', 6D' and 6F'), defined as the length of time between 10% and 90% of the post-stimulus peak-to-peak difference in $\Delta F/F$, and the exponential time constant k defined by $\Delta F/F(t) = ce^{kt}$.

In the text we use "basal calcium signal" to indicate $\Delta F/F$ readings that follow a relatively slow time course and do not appear to be in response to visual stimuli (see Figs 4B, 4C, 5A, 6A and 6B). The $\Delta F/F$ readings that occur during the first sixty seconds of the Figs 5 and 6 experiments ("Epoch 1") prior to changing the perfusion solution are indicated as "baseline" values. The Epoch 1 "baseline" includes values for both the *basal calcium level* and the magnitude of the *calcium transients* seen in response to visual stimuli.

To examine the changes in fluorescence representing changes in basal calcium in visual experiments shown in Fig 6A and 6B responses to the visual stimuli were removed using a series of second-order notch filters at 0.19–0.21 Hz and 0.38–0.42 Hz.

Statistical tests

For (Fig 5C–5C" and 5E–5E") and (Fig 6D–6D" and 6E–6E") comparisons are two-way repeated measure ANOVA (brackets show interactions between time and genotype) and Sidak's multiple comparisons tests, $p \leq 0.05$ *, $p \leq 0.01$ **, $p \leq 0.001$ ***, $p \leq 0.0001$ ****. These tests were performed using Graphpad Prism Software (San Diego, CA). Differences in basal calcium shown in Fig 6A and 6B were calculated by two-tailed Wilcoxon rank sum tests in Matlab R2017a.

Replicates

Each biological replicate (N) represents one fly, except for RT-qPCR and RNA-Seq (Fig 2, and S7E Fig) where each biological replicate was pooled from 18+ flies. RT-qPCR experiments include 3 technical replicates, which are averaged to represent a single biological replicate. Animals from at least 3 crosses were used for each experiment. Data for each experiment was collected over 2–6 months in at least 3 experiments. No outliers were removed from any data set. Live imaging recordings with too much movement were excluded and not analyzed.

Supporting information

S1 Fig. Serotonin receptors and serotonergic projections in the optic lobe. (**A-H**) Serotonin receptor MiMIC-T2A-GAL4 lines were crossed to UAS-mCD8::RFP (visualized here in green) to identify patterns of expression in the optic lobe. (**A**) A schematic of the optic lobe neuropils including the lamina (la), medulla (me), lobula (lo) and lobula plate (lp) with the neuropil in grey and the cortex containing neuronal cell bodies in white. (**B-F**) Neuropil is labeled by anti-N-Cadherin staining (blue) to provide anatomical reference for labeled cells (green) representing 5-HT1A (**B**), 5-HT1B (**C**), 5-HT2A (**D**), 5-HT2B (**E**), and 5-HT7 (**F**). MiMIC-T2A-GAL4 line labeled projections were visible in all optic lobe neuropils including the lamina neuropil,

which is enlarged in (B'), (C'), (E') and (F'). N = 4–8 and scale bars are 20 μm.
(TIF)

S2 Fig. Data sets reporting evidence of serotonin receptor expression in optic lobe neurons.
The current study includes MiMIC-T2A-GAL4>MCFO for identification based on morphology (green) and FACS-SMART-Seq of L2 and T1 neurons (blue). Davis et al. 2020 [70]
employed TAPIN-Seq and reported probability of expression (GSE116969, Table 7B) for each
cell type. Serotonin receptor expression with a p>0.75 are shown (purple). Konstantinides
et al. 2018 [71] used FACS-SMART-Seq for T1, Mi1, C2 and C3 cells (GSE103772). Serotonin
receptors with counts greater than 1,000 in at least two replicates are shown (orange).
(TIF)

**S3 Fig. Serotonin receptor MiMIC-T2A-GAL4 lines potentially label L2, C2, TMY3, and
Mi1 cells.** (**A**) 5-HT2B-MiMIC-T2A-GAL4>UAS-RFP (green) was combined with ChAT-Mi-
MIC-LexA>LexAop-GFP (magenta). Co-labeling was observed in cell bodies in the lamina
cortex, shown in insets (arrowheads). (**B-C**) 5-HT7-MiMIC-T2A-GAL4 labeled cells with a
morphology similar to lamina monopolar cell 5 (L5). (**D**) 5-HT1A-MiMIC-T2A-GAL4>MCFO
labeled C2-like cells in the lamina neuropil. (**E**) Colocalization was observed between 5-HT1A
MiMIC-T2A-GAL4 and GAD1 MiMIC-T2A-LexA in the lamina neuropil and cell bodies adja-
cent to the lobula plate (arrowhead, E). (**F-G**) 5-HT7-MiMIC-GAL4>MCFO (F) and 5-HT1A-
MiMIC-T2A-GAL4>MCFO (G) labeled cells with morphology similar to TmY3. (**H**) 5-HT7-
MiMIC-GAL4>MCFO also labeled cells that resembled Mi1. For co-labeling in (A) and (E),
N = 4–8 brains per condition. For MCFO, L5-like cells in (B-C) were observed in 7/13 brains,
C2 cells in (D) were observed in 3/31 brains, TMY3 cells in (F) were observed in 4/13 brains,
TmY3 cells in (G) were observed in 5/31 brains and Mi1 cells in (H) were observed in 6/13
brains. Scale bars are 20 μm for (A, D-H) and 10 μm for (B-C).
(TIF)

S4 Fig. 5-HT2A labeling in lamina cortex may represent glia cells. (**A**) 5-HT2A-GAL4>
MCFO epitopes V5 (green) and HA (magenta) label unidentified cells confined the distal lam-
ina cortex. (**B**) 5-HT2A-T2A-GAL4>UAS-mCD8::GFP (green) labels cells in the lamina cor-
tex in close proximity to nuclei labeled with repo antibody (magenta). Neuropil is labeled by
anti-N-Cadherin staining (blue) to provide anatomical reference. N = 18 brains for (A) and
N = 4 brains from (B). Scale bars are 20 um.
(TIF)

**S5 Fig. Serotonin receptor 5-HT1B co-labels with serotonin immunoreactive sites in optic
lobe and cell bodies in the central brains.** Anti-serotonin immunolabeling (magenta) was
used to identify serotonergic cells and projections in (A-F). (**A**) Serotonin immunoreactive
sites (magenta) were visible in the optic lobe neuropils: lamina (la), medulla (me), lobula (lo)
and lobula plate (lp). (**B**) A schematic of the optic lobe and its major neuropils. (**A'-A" and
C-C"**) 5-HT1B-MiMIC-T2A-GAL4>UAS-mCD8::GFP labeled cells throughout the optic lobe
with close apposition to serotonergic boutons. A neuron in serotonergic cell cluster LP2 is also
labeled by 5-HT1B driven GFP (arrowhead, A-A"). (D) A schematic of the fly brain with
dashed lines showing the approximate anatomical locations for (C) and (E). (E-E") Serotonin
receptor MiMIC-T2A-GAL4 lines were crossed to UAS-MCFO-1 to label individual cells.
Using 5-HT1B-MiMIC-T2A-GAL4>MCFO (green), we observed co-labeling between
MCFO-labeled cells and serotonergic boutons (magenta) processes in the inner medulla (iM),
medulla layer 4 (M4), and lobula (lo). (F-F") Anti-serotonin immunolabeling (magenta) co-
labeled with 5-HT1B-MiMIC-T2A-GAL4>UAS-mCD8::GFP labeled cell bodies in the central
brain. 5-HT1B-labeled Kenyon cells (KC) are labeled for anatomical reference in (F"). (G) The

approximate anatomical location for images in (F-F") are shown in the boundaries of the dashed line. Serotonin co-labeling was performed N = 5 for 5-HT1B>GFP (A-A", C-C", and F-F") and N = 6 brains for 5-HT1B>MCFO (E-E"). Scale bars are 20 μm.
(TIF)

S6 Fig. Serotonin receptor 5-HT1A co-labels with serotonin immunoreactive sites in optic lobe and cell bodies in the central brain. (**A**) Schematic of the optic lobe neuropils—lamina (la), medulla (me), lobula (lo) and lobula plate (lp)—and serotonergic PLP cells. (**B-B"**) 5-HT1A-MiMIC-T2A-GAL4 driving UAS-mCD8::GFP (green) was co-stained with anti-sero-tonin immunolabeling (magenta) to map potential autoreceptors to specific cell clusters in the central brain. PLP neurons co-labeling for 5-HT1A labeling and anti-serotonin immunolabel-ing are indicated by the arrowhead. (**C-E**) Anterior to posterior images taken in the same brain show several serotonergic cell clusters expressing 5-HT1A (labeled at arrowheads). 5-HT1A-labeled mushroom body (MB) and kenyon cells (KC) are labeled for anatomical ref-erence in (**C** and **E**). (**F**) A cartoon of the fly brain with dashed lines to indicate the approxi-mate anatomical location for (C-E). Scale bars are 20 μm and N = 6.
(TIF)

S7 Fig. RT-qPCR shows L2 neurons express 5-HT2B and T1 neurons express both 5-HT1A and 5-HT1B serotonin receptors. Enrichment (i.e., fold change) was calculated for cDNA from GFP-labeled cell isolates relative to pooled, unlabeled optic lobe cell isolates using the comparative CT method. The dotted line indicates y = 1. Values >1 signify that the transcript is more abundant (enriched) in GFP-labeled cells, while values <1 signify that these transcripts are less abundant in GFP-labeled cells A zero value was imputed for samples with no detectable transcript amplification (i.e., no CT value). (**A**) RT-qPCR performed on cDNA from isolated T1 neurons expressing GFP showed enrichment for serotonin receptors 5-HT1A and 5-HT1B relative to other GFP-negative cells from the optic lobe. (**B**) FACS isolates from L2 cells showed enrichment of 5-HT2B and 5-HT7 in RT-qPCR. (**C**) L1 RT-qPCR enrichment was not detectable for any serotonin receptors. RT-qPCR error bars represent mean±SEM. N = 3–6 biological replicates pooled from 18–40 brains per replicate.
(TIF)

S8 Fig. Serotonergic neurons do not show sybGRASP signal with postsynaptic T1, L2 or L1 neurons in the medulla. SybGRASP was used to probe whether serotonergic neurons make synaptic contacts onto L2, T1 or L1 neurons. L2 neurons are known to synapse onto T1 projec-tions in the medulla and we used this connection as a positive control. (**A-A'**) SybGRASP was observed with L2 split-GAL4 presynaptic to T1-LexA in M2. The dashed inset in (**A**) is shown in (**A'**). (**B-E**) A SerT-GAL4 driver was used to express the pre-synaptic portion of GFP in serotonergic neurons and LexA drivers were used to express the postsynaptic portion of GFP in L2 (**B-C**) L1 (**D**) or T1 (**E**) as indicated. No sybGRASP signal was detected in the medulla when SerT was presynaptic to L2 (**B**) however, occasional sparse GFP puncta (arrowhead) were visible in the lamina (**C**). When SerT-GAL4 neurons were presynaptic to L1 (**D**) or T1 (**E**) neurons, we did not detect a sybGRASP signal in either the lamina or medulla. All tissue was labeled with primary antibodies to both 5-HT (magenta) and GFP (green). N = 7–10 brains. Scale bars are 15 μm (**A**, **B**, **D-E**); 5 μm (**A"** and **C-C"**).
(TIF)

S9 Fig. Individual traces for serotonin bath application experiments. (**A-D**) Individual traces representing all experiments (Fig 4) for serotonin or saline controls with L2, L1 or T1 split-GAL4>GCaMP6f or T1 split-GAL4>ArcLight. For all experiments, the first 60 s of the recording is not shown; traces represent data recorded following a switch to saline with

serotonin or saline alone. The length of time for the switch to complete was estimated to be 105 s, but the first 60 s of the recording are not shown so the switch occurs at 45 s on the x axis in A-D. Saline controls are gray, serotonin exposed preps are colored, and the dark line represents the mean. (**A**) L2>GCaMP6f experiments, along with (**B**) L1>GCaMP6f, show an increase in calcium following serotonin application as compared to saline controls (L2, p = 00095; L1, p = 0.02). (**C, D**) T1 cells show no significant change with either GCaMP6f (**C**) or ArcLight (**D**) relative to saline (p>0.05) For bath application experiments (**A-D**), N = 4–8 individual flies.
(TIF)

S10 Fig. Additional Analysis of visually induced calcium transients in Fig 5. Visually induced calcium transients were recorded in flies expressing L2-split-GAL4>GCaMP6f as in Fig 5. Bath application with saline followed by saline (blue) or serotonin (red) at 105 s. Analysis of visual stimuli response. For plotting each variable, the average value for the epoch 1 baseline was subtracted; epoch 1 is therefore always set to 0. (**A**) The change in the secondary response (the magnitude of the calcium decrease following the initial peak). (**B**) Change in the exponential time constant k (units 1/sec) relative to epoch 1 (defined by $\Delta F/F(t) = ce^{kt}$) for the time between 10% and 90% of the post-stimulus peak-to-peak difference in $\Delta F/F$. (**C**) Change in the secondary calcium response (the magnitude of the calcium increase following the initial trough). (**D**) Change in the exponential time constant relative to epoch 1. N = 14 and N = 20 individual flies perfused with serotonin or saline respectively. Shaded areas show mean +/- SEM.
(TIF)

S11 Fig. Additional Analysis of visually induced calcium transients in Fig 6. Visually induced calcium transients were recorded in 5-HT2B +/- or 5-HT2B -/- flies as described in Fig 6. (**A**) The change in the secondary response (the magnitude of the calcium decrease following the initial peak). (**B**) Change in the exponential time constant k (units 1/sec) relative to epoch 1 (defined by $\Delta F/F(t) = ce^{kt}$) for the time between 10% and 90% of the post-stimulus peak-to-peak difference in $\Delta F/F$. (**C**) Change in the secondary calcium response (the magnitude of the calcium increase following the initial trough). (**D**) Change in the exponential time constant relative to epoch 1. N = 13 5-HT2B +/- and N = 15 5-HT2B -/- flies, all receiving serotonin, were tested. Shaded areas show mean +/- SEM. Comparisons in are two-way repeated measures ANOVA (brackets show interaction of time and genotype) and Sidak's multiple comparisons tests for indicated time points, $p \leq 0.05^*$.
(TIF)

S1 Table. RNA-Seq Serotonin Receptor TPMs, averages and standard deviations.
(PDF)

S2 Table. RT-qPCR Threshold Cycle (CT) measurements and calculated enrichment for FACS-isolated T1, L2, and L1 samples as shown in S7 Fig. Enrichment (i.e., fold change) was calculated for cDNA from GFP-labeled cell isolates relative to pooled, unlabeled optic lobe cell isolates using the comparative CT method.
(PDF)

S3 Table. Fly strains used in this study.
(PDF)

S4 Table. RT-qPCR primer sequences and mRNA (cDNA) target information.
(PDF)

Acknowledgments

Author Contributions

Conceptualization: Mark A. Frye, David E. Krantz.

Data curation: Maureen M. Sampson, Ben J. Hardcastle, Shivan L. Bonanno.

Formal analysis: Maureen M. Sampson, Katherine M. Myers Gschweng, Ben J. Hardcastle, Shivan L. Bonanno, Fuying Gao.

Funding acquisition: Maureen M. Sampson, Tyler R. Sizemore, Andrew M. Dacks, Mark A. Frye, David E. Krantz.

Investigation: Maureen M. Sampson, Katherine M. Myers Gschweng, Ben J. Hardcastle, Shivan L. Bonanno, Tyler R. Sizemore, Fuying Gao.

Methodology: Maureen M. Sampson, Katherine M. Myers Gschweng, Ben J. Hardcastle, Shivan L. Bonanno, Mark A. Frye.

Project administration: Mark A. Frye, David E. Krantz.

Resources: Andrew M. Dacks, David E. Krantz.

Software: Ben J. Hardcastle.

Supervision: Andrew M. Dacks, Mark A. Frye, David E. Krantz.

Validation: Maureen M. Sampson, Katherine M. Myers Gschweng, Ben J. Hardcastle, Rebecca C. Arnold.

Visualization: Katherine M. Myers Gschweng, Tyler R. Sizemore.

Writing – original draft: Maureen M. Sampson, Katherine M. Myers Gschweng, David E. Krantz.

Writing – review & editing: Maureen M. Sampson, Katherine M. Myers Gschweng, Ben J. Hardcastle, Shivan L. Bonanno, Tyler R. Sizemore, Andrew M. Dacks, Mark A. Frye, David E. Krantz.

References

1. Kupfermann I. Modulatory actions of neurotransmitters. Annual review of neuroscience. 1979; 2:447–65. https://doi.org/10.1146/annurev.ne.02.030179.002311 PMID: 44174

2. Marder E. Neuromodulation of neuronal circuits: back to the future. Neuron. 2012; 76(1):1–11. https://doi.org/10.1016/j.neuron.2012.09.010 PMID: 23040802

3. Marder E, O'Leary T, Shruti S. Neuromodulation of circuits with variable parameters: single neurons and small circuits reveal principles of state-dependent and robust neuromodulation. Annual review of neuroscience. 2014; 37:329–46. https://doi.org/10.1146/annurev-neuro-071013-013958 PMID: 25032499

4. Nadim F, Bucher D. Neuromodulation of neurons and synapses. Current opinion in neurobiology. 2014; 29:48–56. https://doi.org/10.1016/j.conb.2014.05.003 PMID: 24907657

5. Katz PS. Beyond Neurotransmission: Neuromodulation and its Importance for Information Processing. Oxford; New York: Oxford University Press; 1999. xiii, 391 p. p.

6. Moreau AW, Amar M, Le Roux N, Morel N, Fossier P. Serotoninergic fine-tuning of the excitation-inhibition balance in rat visual cortical networks. Cereb cortex. 2010; 20(2):456–67. https://doi.org/10.1093/cercor/bhp114 PMID: 19520765

7. Arechiga H, Banuelos E, Frixione E, Picones A, Rodriguez-Sosa L. Modulation of crayfish retinal sensitivity by 5-hydroxytryptamine. The Journal of experimental biology. 1990; 150:123–43. PMID: 2355208

8. Seillier L, Lorenz C, Kawaguchi K, Ott T, Nieder A, Pourriahi P, et al. Serotonin Decreases the Gain of Visual Responses in Awake Macaque V1. The Journal of neuroscience: the official journal of the Society for Neuroscience. 2017; 37(47):11390–405.

9. Kloppenburg P, Ferns D, Mercer AR. Serotonin enhances central olfactory neuron responses to female sex pheromone in the male sphinx moth manduca sexta. The Journal of neuroscience: the official journal of the Society for Neuroscience. 1999; 19(19):8172–81.

10. Dacks AM, Christensen TA, Hildebrand JG. Modulation of olfactory information processing in the antennal lobe of Manduca sexta by serotonin. Journal of neurophysiology. 2008; 99(5):2077–85. https://doi.org/10.1152/jn.01372.2007 PMID: 18322001

11. Lottem E, Lorincz ML, Mainen ZF. Optogenetic Activation of Dorsal Raphe Serotonin Neurons Rapidly Inhibits Spontaneous But Not Odor-Evoked Activity in Olfactory Cortex. The Journal of neuroscience: the official journal of the Society for Neuroscience. 2016; 36(1):7–18.

12. Brunert D, Tsuno Y, Rothermel M, Shipley MT, Wachowiak M. Cell-Type-Specific Modulation of Sensory Responses in Olfactory Bulb Circuits by Serotonergic Projections from the Raphe Nuclei. The Journal of neuroscience: the official journal of the Society for Neuroscience. 2016; 36(25):6820–35.

13. Petzold GC, Hagiwara A, Murthy VN. Serotonergic modulation of odor input to the mammalian olfactory bulb. Nature neuroscience. 2009; 12(6):784–91. https://doi.org/10.1038/nn.2335 PMID: 19430472

14. Papesh MA, Hurley LM. Modulation of auditory brainstem responses by serotonin and specific serotonin receptors. Hearing research. 2016; 332:121–36. https://doi.org/10.1016/j.heares.2015.11.014 PMID: 26688176

15. Fotowat H, Harvey-Girard E, Cheer JF, Krahe R, Maler L. Subsecond Sensory Modulation of Serotonin Levels in a Primary Sensory Area and Its Relation to Ongoing Communication Behavior in a Weakly Electric Fish. eNeuro. 2016; 3(5).

16. Andres M, Seifert M, Spalthoff C, Warren B, Weiss L, Giraldo D, et al. Auditory Efferent System Modulates Mosquito Hearing. Current biology: CB. 2016; 26(15):2028–36. https://doi.org/10.1016/j.cub.2016.05.077 PMID: 27476597

17. Watakabe A, Komatsu Y, Sadakane O, Shimegi S, Takahata T, Higo N, et al. Enriched expression of serotonin 1B and 2A receptor genes in macaque visual cortex and their bidirectional modulatory effects on neuronal responses. Cereb cortex. 2009; 19(8):1915–28. https://doi.org/10.1093/cercor/bhn219 PMID: 19056862

18. Gagolewicz PJ, Dringenberg HC. Age-Dependent Switch of the Role of Serotonergic 5-HT1A Receptors in Gating Long-Term Potentiation in Rat Visual Cortex In Vivo. Neural plast. 2016; 2016:6404082. https://doi.org/10.1155/2016/6404082 PMID: 27247804

19. Lombaert N, Hennes M, Gilissen S, Schevenels G, Aerts L, Vanlaer R, et al. 5-HTR2A and 5-HTR3A but not 5-HTR1A antagonism impairs the cross-modal reactivation of deprived visual cortex in adulthood. Mol brain. 2018; 11(1):65. https://doi.org/10.1186/s13041-018-0404-5 PMID: 30400993

20. Gu Q, Singer W. Involvement of serotonin in developmental plasticity of kitten visual cortex. Eur J Neurosci. 1995; 7(6):1146–53. https://doi.org/10.1111/j.1460-9568.1995.tb01104.x PMID: 7582087

21. Wang Y, Gu Q, Cynader MS. Blockade of serotonin-2C receptors by mesulergine reduces ocular dominance plasticity in kitten visual cortex. Exp brain res. 1997; 114(2):321–8. https://doi.org/10.1007/pl00005640 PMID: 9166921

22. Shimegi S, Kimura A, Sato A, Aoyama C, Mizuyama R, Tsunoda K, et al. Cholinergic and serotonergic modulation of visual information processing in monkey V1. Journal of physiology, Paris. 2016; 110(1–2):44–51. https://doi.org/10.1016/j.jphysparis.2016.09.001 PMID: 27619519

23. Zhou X, Zhang R, Zhang S, Wu J, Sun X. Activation of 5-HT1A receptors promotes retinal ganglion cell function by inhibiting the cAMP-PKA pathway to modulate presynaptic GABA release in chronic glaucoma. The Journal of neuroscience: the official journal of the Society for Neuroscience. 2018.

24. Trakhtenberg EF, Pita-Thomas W, Fernandez SG, Patel KH, Venugopalan P, Shechter JM, et al. Serotonin receptor 2C regulates neurite growth and is necessary for normal retinal processing of visual

information. Developmental neurobiology. 2017; 77(4):419–37. https://doi.org/10.1002/dneu.22391 PMID: 26999672

25. Borst A, Helmstaedter M. Common circuit design in fly and mammalian motion vision. Nature neuroscience. 2015; 18(8):1067–76. https://doi.org/10.1038/nn.4050 PMID: 26120965

26. Cheng KY, Frye MA. Neuromodulation of insect motion vision. Journal of comparative physiology A, Neuroethology, sensory, neural, and behavioral physiology. 2019.

27. Meinertzhagen IA, O'Neil SD. Synaptic organization of columnar elements in the lamina of the wild type in Drosophila melanogaster. The Journal of comparative neurology. 1991; 305(2):232–63. https://doi.org/10.1002/cne.903050206 PMID: 1902848

28. Joesch M, Schnell B, Raghu SV, Reiff DF, Borst A. ON and OFF pathways in Drosophila motion vision. Nature. 2010; 468(7321):300–4. https://doi.org/10.1038/nature09545 PMID: 21068841

29. Strother JA, Nern A, Reiser MB. Direct observation of ON and OFF pathways in the Drosophila visual system. Current biology: CB. 2014; 24(9):976–83. https://doi.org/10.1016/j.cub.2014.03.017 PMID: 24704075

30. Clark DA, Bursztyn L, Horowitz MA, Schnitzer MJ, Clandinin TR. Defining the computational structure of the motion detector in Drosophila. Neuron. 2011; 70(6):1165–77. https://doi.org/10.1016/j.neuron.2011.05.023 PMID: 21689602

31. Yang HH, St-Pierre F, Sun X, Ding X, Lin MZ, Clandinin TR. Subcellular Imaging of Voltage and Calcium Signals Reveals Neural Processing In Vivo. Cell. 2016; 166(1):245–57. https://doi.org/10.1016/j.cell.2016.05.031 PMID: 27264607

32. Zheng L, de Polavieja GG, Wolfram V, Asyali MH, Hardie RC, Juusola M. Feedback network controls photoreceptor output at the layer of first visual synapses in Drosophila. The Journal of general physiology. 2006; 127(5):495–510. https://doi.org/10.1085/jgp.200509470 PMID: 16636201

33. Behnia R, Desplan C. Visual circuits in flies: beginning to see the whole picture. Current opinion in neurobiology. 2015; 34:125–32. https://doi.org/10.1016/j.conb.2015.03.010 PMID: 25881091

34. Bahl A, Serbe E, Meier M, Ammer G, Borst A. Neural Mechanisms for Drosophila Contrast Vision. Neuron. 2015; 88(6):1240–52. https://doi.org/10.1016/j.neuron.2015.11.004 PMID: 26673659

35. Rivera-Alba M, Vitaladevuni SN, Mishchenko Y, Lu Z, Takemura SY, Scheffer L, et al. Wiring economy and volume exclusion determine neuronal placement in the Drosophila brain. Current biology: CB. 2011; 21(23):2000–5. https://doi.org/10.1016/j.cub.2011.10.022 PMID: 22119527

36. Takemura SY, Lu Z, Meinertzhagen IA. Synaptic circuits of the Drosophila optic lobe: the input terminals to the medulla. The Journal of comparative neurology. 2008; 509(5):493–513. https://doi.org/10.1002/cne.21757 PMID: 18537121

37. Takemura SY, Bharioke A, Lu Z, Nern A, Vitaladevuni S, Rivlin PK, et al. A visual motion detection circuit suggested by Drosophila connectomics. Nature. 2013; 500(7461):175–81. https://doi.org/10.1038/nature12450 PMID: 23925240

38. Takemura SY, Xu CS, Lu Z, Rivlin PK, Parag T, Olbris DJ, et al. Synaptic circuits and their variations within different columns in the visual system of Drosophila. Proceedings of the National Academy of Sciences of the United States of America. 2015; 112(44):13711–6. https://doi.org/10.1073/pnas.1509820112 PMID: 26483464

39. Takemura SY, Nern A, Chklovskii DB, Scheffer LK, Rubin GM, Meinertzhagen IA. The comprehensive connectome of a neural substrate for 'ON' motion detection in. Elife. 2017;6.

40. Shinomiya K, Huang G, Lu Z, Parag T, Xu CS, Aniceto R, et al. Comparisons between the ON- and OFF-edge motion pathways in the Drosophila brain. Elife. 2019;8.

41. Wasserman SM, Aptekar JW, Lu P, Nguyen J, Wang AL, Keles MF, et al. Olfactory neuromodulation of motion vision circuitry in Drosophila. Current biology: CB. 2015; 25(4):467–72. https://doi.org/10.1016/j.cub.2014.12.012 PMID: 25619767

42. Strother JA, Wu ST, Rogers EM, Eliason JLM, Wong AM, Nern A, et al. Behavioral state modulates the ON visual motion pathway of Drosophila. Proceedings of the National Academy of Sciences of the United States of America. 2018; 115(1):E102–E11. https://doi.org/10.1073/pnas.1703090115 PMID: 29255026

43. Cheng KY, Colbath RA, Frye MA. Olfactory and Neuromodulatory Signals Reverse Visual Object Avoidance to Approach in Drosophila. Current biology: CB. 2019; 29(12):2058–65 e2. https://doi.org/10.1016/j.cub.2019.05.010 PMID: 31155354

44. Hevers W, Hardie RC. Serotonin modulates the voltage dependence of delayed rectifier and Shaker potassium channels in Drosophila photoreceptors. Neuron. 1995; 14:845–56. https://doi.org/10.1016/0896-6273(95)90228-7 PMID: 7718246

45. Kloppenburg P, Erber J. The modulatory effects of serotonin and octopamine in the visual system of the honey bee (Apis mellifera L.) II. Electrophysiological analysis of motion-sensitive neurons in the

lobula. Journal of comparative physiology A, Neuroethology, sensory, neural, and behavioral physiology. 1995; 176:119–29.

46. Suver MP, Mamiya A, Dickinson MH. Octopamine neurons mediate flight-induced modulation of visual processing in Drosophila. Current biology: CB. 2012; 22(24):2294–302. https://doi.org/10.1016/j.cub.2012.10.034 PMID: 23142045

47. Leitinger G, Pabst MA, Kral K. Serotonin-immunoreactive neurones in the visual system of the praying mantis: an immunohistochemical, confocal laser scanning and electron microscopic study. Brain res. 1999; 823(1–2):11–23. https://doi.org/10.1016/s0006-8993(98)01339-0 PMID: 10095007

48. Nässel DR, Meyer EP, Klemm N. Mapping and ultrastructure of serotonin-immunoreactive neurons in the optic lobes of three insect species. The Journal of comparative neurology. 1985; 232(2):190–204. https://doi.org/10.1002/cne.902320205 PMID: 3973090

49. Nässel DR, Ohlsson L, Sivasubramanian P. Postembryonic differentiation of serotonin-immunoreactive neurons in fleshfly optic lobes developing in situ or cultured in vivo without eye discs. The Journal of comparative neurology. 1987; 255(3):327–40. https://doi.org/10.1002/cne.902550302 PMID: 3546409

50. Valles AM, White K. Serotonin-containing neurons in Drosophila melanogaster: development and distribution. The Journal of comparative neurology. 1988; 268(3):414–28. https://doi.org/10.1002/cne.902680310 PMID: 3129459

51. Hamanaka Y, Kinoshita M, Homberg U, Arikawa K. Immunocytochemical localization of amines and GABA in the optic lobe of the butterfly, Papilio xuthus. PloS one. 2012; 7(7):e41109. https://doi.org/10.1371/journal.pone.0041109 PMID: 22844431

52. Schafer S, Bicker G. Common projection areas of 5-HT- and GABA-like immunoreactive fibers in the visual system of the honeybee. Brain res. 1986; 380(2):368–70. https://doi.org/10.1016/0006-8993(86)90237-4 PMID: 3530374

53. Chen B, Meinertzhagen IA, Shaw SR. Circadian rhythms in light-evoked responses of the fly's compound eye, and the effects of neuromodulators 5-HT and the peptide PDF. J comp physiol [A]. 1999; 185:393–404.

54. Ichikawa T. Light suppresses the activity of serotonin-immunoreactive neurons in the optic lobe of the swallowtail butterfly. Neurosci lett. 1994; 172(1–2):115–8. https://doi.org/10.1016/0304-3940(94)90675-0 PMID: 8084513

55. Nichols CD. 5-HT2 receptors in Drosophila are expressed in the brain and modulate aspects of circadian behaviors. Developmental neurobiology. 2007; 67(6):752–63. https://doi.org/10.1002/dneu.20370 PMID: 17443822

56. Yuan Q, Lin F, Zheng X, Sehgal A. Serotonin modulates circadian entrainment in Drosophila. Neuron. 2005; 47(1):115–27. https://doi.org/10.1016/j.neuron.2005.05.027 PMID: 15996552

57. Helfrich-Forster C. Light input pathways to the circadian clock of insects with an emphasis on the fruit fly Drosophila melanogaster. Journal of comparative physiology A, Neuroethology, sensory, neural, and behavioral physiology. 2020; 206(2):259–72. https://doi.org/10.1007/s00359-019-01379-5 PMID: 31691095

58. Helfrich-Forster C, Winter C, Hofbauer A, Hall JC, Stanewsky R. The circadian clock of fruit flies is blind after elimination of all known photoreceptors. Neuron. 2001; 30(1):249–61. https://doi.org/10.1016/s0896-6273(01)00277-x PMID: 11343659

59. Pyza E, Meinertzhagen IA. Neurotransmitters regulate rhythmic size changes amongst cells in the fly's optic lobe. Journal of comparative physiology A, Sensory, neural, and behavioral physiology. 1996; 178(1):33–45. https://doi.org/10.1007/BF00189588 PMID: 8568723

60. Tomioka K, Ikeda M, Nagao T, Tamotsu S. Involvement of serotonin in the circadian rhythm of an insect visual system. Naturwissenschaften. 1993; 80(3):137–9.

61. Nichols DE, Nichols CD. Serotonin receptors. Chemical reviews. 2008; 108(5):1614–41. https://doi.org/10.1021/cr078224o PMID: 18476671

62. McCorvy JD, Roth BL. Structure and function of serotonin G protein-coupled receptors. Pharmacology & therapeutics. 2015; 150:129–42.

63. Maroteaux L, Bechade C, Roumier A. Dimers of serotonin receptors: Impact on ligand affinity and signaling. Biochimie. 2019; 161:23–33. https://doi.org/10.1016/j.biochi.2019.01.009 PMID: 30685449

64. Araneda R, Andrade R. 5-Hydroxytryptamine2 and 5-hydroxytryptamine 1A receptors mediate opposing responses on membrane excitability in rat association cortex. Neuroscience. 1991; 40(2):399–412. https://doi.org/10.1016/0306-4522(91)90128-b PMID: 1851255

65. Celada P, Puig MV, Artigas F. Serotonin modulation of cortical neurons and networks. Frontiers in integrative neuroscience. 2013; 7:25. https://doi.org/10.3389/fnint.2013.00025 PMID: 23626526

66. Elliott MC, Tanaka PM, Schwark RW, Andrade R. Serotonin Differentially Regulates L5 Pyramidal Cell Classes of the Medial Prefrontal Cortex in Rats and Mice. eNeuro. 2018;5(1).

67. Llado-Pelfort L, Santana N, Ghisi V, Artigas F, Celada P. 5-HT1A receptor agonists enhance pyramidal cell firing in prefrontal cortex through a preferential action on GABA interneurons. Cereb cortex. 2012; 22(7):1487–97. https://doi.org/10.1093/cercor/bhr220 PMID: 21893679

68. Gao M, Der-Ghazarian TS, Li S, Qiu S, Neisewander JL, Wu J. Dual Effect of 5-HT1B/1D Receptors on Dopamine Neurons in Ventral Tegmental Area: Implication for the Functional Switch After Chronic Cocaine Exposure. Biol psychiatry. 2020.

69. Del Rosario JS, Yudin Y, Su S, Hartle CM, Mirshahi T, Rohacs T. Gi-coupled receptor activation potentiates Piezo2 currents via Gbetagamma. EMBO Rep. 2020; 21(5):e49124. https://doi.org/10.15252/embr.201949124 PMID: 32227462

70. Davis FP, Nern A, Picard S, Reiser MB, Rubin GM, Eddy SR, et al. A genetic, genomic, and computational resource for exploring neural circuit function. Elife. 2020;9.

71. Konstantinides N, Kapuralin K, Fadil C, Barboza L, Satija R, Desplan C. Phenotypic Convergence: Distinct Transcription Factors Regulate Common Terminal Features. Cell. 2018; 174(3):622–35 e13. https://doi.org/10.1016/j.cell.2018.05.021 PMID: 29909983

72. Colas JF, Launay JM, Kellermann O, Rosay P, Maroteaux L. Drosophila 5-HT2 serotonin receptor: coexpression with fushi-tarazu during segmentation. Proceedings of the National Academy of Sciences of the United States of America. 1995; 92(12):5441–5. https://doi.org/10.1073/pnas.92.12.5441 PMID: 7777527

73. Gasque G, Conway S, Huang J, Rao Y, Vosshall LB. Small molecule drug screening in Drosophila identifies the 5HT2A receptor as a feeding modulation target. Scientific reports. 2013; 3:srep02120. https://doi.org/10.1038/srep02120 PMID: 23817146

74. Saudou F, Boschert U, Amlaiky N, Plassat JL, Hen R. A family of Drosophila serotonin receptors with distinct intracellular signalling properties and expression patterns. The EMBO journal. 1992; 11(1):7–17. PMID: 1310937

75. Witz P, Amlaiky N, Plassat JL, Maroteaux L, Borrelli E, Hen R. Cloning and characterization of a Drosophila serotonin receptor that activates adenylate cyclase. Proceedings of the National Academy of Sciences of the United States of America. 1990; 87(22):8940–4. https://doi.org/10.1073/pnas.87.22.8940 PMID: 2174167

76. Blenau W, Daniel S, Balfanz S, Thamm M, Baumann A. Dm5-HT2B: Pharmacological Characterization of the Fifth Serotonin Receptor Subtype of Drosophila melanogaster. Front syst neurosci. 2017; 11:28. https://doi.org/10.3389/fnsys.2017.00028 PMID: 28553207

77. Gnerer JP, Venken KJ, Dierick HA. Gene-specific cell labeling using MiMIC transposons. Nucleic acids research. 2015; 43(8):e56. https://doi.org/10.1093/nar/gkv113 PMID: 25712101

78. Venken KJ, Schulze KL, Haelterman NA, Pan H, He Y, Evans-Holm M, et al. MiMIC: a highly versatile transposon insertion resource for engineering Drosophila melanogaster genes. Nature methods. 2011; 8(9):737–43. https://doi.org/10.1038/nmeth.1662 PMID: 21985007

79. Diao F, Ironfield H, Luan H, Shropshire WC, Ewer J, Marr E, et al. Plug-and-play genetic access to drosophila cell types using exchangeable exon cassettes. Cell rep. 2015; 10(8):1410–21. https://doi.org/10.1016/j.celrep.2015.01.059 PMID: 25732830

80. Fischbach KF, Dittrich APM. The optic lobe of Drosophila melanogaster. I. A Golgi analysis of wild type structure. Cell tissue res. 1989; 258:441–75.

81. Sanes JR, Zipursky SL. Design principles of insect and vertebrate visual systems. Neuron. 2010; 66 (1):15–36. https://doi.org/10.1016/j.neuron.2010.01.018 PMID: 20399726

82. Nern A, Pfeiffer BD, Rubin GM. Optimized tools for multicolor stochastic labeling reveal diverse stereotyped cell arrangements in the fly visual system. Proceedings of the National Academy of Sciences of the United States of America. 2015; 112(22):E2967–76. https://doi.org/10.1073/pnas.1506763112 PMID: 25964354

83. Edwards TN, Meinertzhagen IA. The functional organisation of glia in the adult brain of Drosophila and other insects. Progress in neurobiology. 2010; 90(4):471–97. https://doi.org/10.1016/j.pneurobio.2010.01.001 PMID: 20109517

84. DeSalvo MK, Hindle SJ, Rusan ZM, Orng S, Eddison M, Halliwill K, et al. The Drosophila surface glia transcriptome: evolutionary conserved blood-brain barrier processes. Front neurosci. 2014; 8:346. https://doi.org/10.3389/fnins.2014.00346 PMID: 25426014

85. Nässel DR. Serotonin and serotonin-immunoreactive neurons in the nervous system of insects. Progress in neurobiology. 1988; 30(1):1–85. https://doi.org/10.1016/0301-0082(88)90002-0 PMID: 3275407

86. Xu L, He J, Kaiser A, Graber N, Schlager L, Ritze Y, et al. A Single Pair of Serotonergic Neurons Counteracts Serotonergic Inhibition of Ethanol Attraction in Drosophila. PloS one. 2016; 11(12):e0167518. https://doi.org/10.1371/journal.pone.0167518 PMID: 27936023

87. Pooryasin A, Fiala A. Identified Serotonin-Releasing Neurons Induce Behavioral Quiescence and Suppress Mating in Drosophila. The Journal of neuroscience: the official journal of the Society for Neuroscience. 2015; 35(37):12792–812.

88. Sitaraman D, Zars M, Laferriere H, Chen YC, Sable-Smith A, Kitamoto T, et al. Serotonin is necessary for place memory in Drosophila. Proceedings of the National Academy of Sciences of the United States of America. 2008; 105(14):5579–84. https://doi.org/10.1073/pnas.0710168105 PMID: 18385379

89. Alekseyenko OV, Chan YB, Okaty BW, Chang Y, Dymecki SM, Kravitz EA. Serotonergic Modulation of Aggression in Drosophila Involves GABAergic and Cholinergic Opposing Pathways. Current biology: CB. 2019; 29(13):2145–56 e5. https://doi.org/10.1016/j.cub.2019.05.070 PMID: 31231050

90. Tuthill JC, Nern A, Holtz SL, Rubin GM, Reiser MB. Contributions of the 12 neuron classes in the fly lamina to motion vision. Neuron. 2013; 79(1):128–40. https://doi.org/10.1016/j.neuron.2013.05.024 PMID: 23849200

91. Schmittgen TD, Livak KJ. Analyzing real-time PCR data by the comparative C(T) method. Nature protocols. 2008; 3(6):1101–8. https://doi.org/10.1038/nprot.2008.73 PMID: 18546601

92. Deng B, Li Q, Liu X, Cao Y, Li B, Qian Y, et al. Chemoconnectomics: Mapping Chemical Transmission in Drosophila. Neuron. 2019; 101(5):876–93 e4. https://doi.org/10.1016/j.neuron.2019.01.045 PMID: 30799021

93. Qian Y, Cao Y, Deng B, Yang G, Li J, Xu R, et al. Sleep homeostasis regulated by 5HT2b receptor in a small subset of neurons in the dorsal fan-shaped body of drosophila. Elife. 2017;6.

94. Macpherson LJ, Zaharieva EE, Kearney PJ, Alpert MH, Lin TY, Turan Z, et al. Dynamic labelling of neural connections in multiple colours by trans-synaptic fluorescence complementation. Nat commun. 2015; 6:10024. https://doi.org/10.1038/ncomms10024 PMID: 26635273

95. Trueta C, De-Miguel FF. Extrasynaptic exocytosis and its mechanisms: a source of molecules mediating volume transmission in the nervous system. Frontiers in physiology. 2012; 3:319. https://doi.org/10.3389/fphys.2012.00319 PMID: 22969726

96. Bunin MA, Wightman RM. Paracrine neurotransmission in the CNS: involvement of 5-HT. Trends neurosci. 1999; 22(9):377–82. https://doi.org/10.1016/s0166-2236(99)01410-1 PMID: 10441294

97. Vizi ES, Fekete A, Karoly R, Mike A. Non-synaptic receptors and transporters involved in brain functions and targets of drug treatment. British journal of pharmacology. 2010; 160(4):785–809. https://doi.org/10.1111/j.1476-5381.2009.00624.x PMID: 20136842

98. Fuxe K, Dahlstrom AB, Jonsson G, Marcellino D, Guescini M, Dam M, et al. The discovery of central monoamine neurons gave volume transmission to the wired brain. Progress in neurobiology. 2010; 90(2):82–100. https://doi.org/10.1016/j.pneurobio.2009.10.012 PMID: 19853007

99. Liu C, Meng Z, Wiggin TD, Yu J, Reed ML, Guo F, et al. A Serotonin-Modulated Circuit Controls Sleep Architecture to Regulate Cognitive Function Independent of Total Sleep in Drosophila. Current biology: CB. 2019; 29(21):3635–46 e5. https://doi.org/10.1016/j.cub.2019.08.079 PMID: 31668619

100. Zhang X, Gaudry Q. Functional integration of a serotonergic neuron in the Drosophila antennal lobe. Elife. 2016;5.

101. Hoyer D, Hannon JP, Martin GR. Molecular, pharmacological and functional diversity of 5-HT receptors. Pharmacol biochem behav. 2002; 71(4):533–54. https://doi.org/10.1016/s0091-3057(01)00746-8 PMID: 11888546

102. Chen TW, Wardill TJ, Sun Y, Pulver SR, Renninger SL, Baohan A, et al. Ultrasensitive fluorescent proteins for imaging neuronal activity. Nature. 2013; 499(7458):295–300. https://doi.org/10.1038/nature12354 PMID: 23868258

103. Narahashi T. Tetrodotoxin: a brief history. Proc Jpn Acad ser B Phys biol sci. 2008; 84(5):147–54. https://doi.org/10.2183/pjab.84.147 PMID: 18941294

104. Narahashi T, Moore JW, Scott WR. Tetrodotoxin Blockage of Sodium Conductance Increase in Lobster Giant Axons. The Journal of general physiology. 1964; 47:965–74. https://doi.org/10.1085/jgp.47.5.965 PMID: 14155438

105. Polter AM, Li X. 5-HT1A receptor-regulated signal transduction pathways in brain. Cell signal. 2010; 22(10):1406–12. https://doi.org/10.1016/j.cellsig.2010.03.019 PMID: 20363322

106. Cao G, Platisa J, Pieribone VA, Raccuglia D, Kunst M, Nitabach MN. Genetically targeted optical electrophysiology in intact neural circuits. Cell. 2013; 154(4):904–13. https://doi.org/10.1016/j.cell.2013.07.027 PMID: 23932121

107. Laughlin SB, Osorio D. Mechanisms for Neural Signal Enhancement in the Blowfly Compound Eye. Journal of experimental biology. 1989; 144(1):113–46.

108. Reiff DF, Plett J, Mank M, Griesbeck O, Borst A. Visualizing retinotopic half-wave rectified input to the motion detection circuitry of Drosophila. Nature neuroscience. 2010; 13(8):973–8. https://doi.org/10.1038/nn.2595 PMID: 20622873

109. Fisher YE, Yang HH, Isaacman-Beck J, Xie M, Gohl DM, Clandinin TR. FlpStop, a tool for conditional gene control in Drosophila. Elife. 2017;6.

110. Kolodziejczyk A, Sun X, Meinertzhagen IA, Nassel DR. Glutamate, GABA and acetylcholine signaling components in the lamina of the Drosophila visual system. PloS one. 2008; 3(5):e2110. https://doi.org/10.1371/journal.pone.0002110 PMID: 18464935

111. Hong CS, Ganetzky B. Spatial and temporal expression patterns of two sodium channel genes in Drosophila. The Journal of neuroscience: the official journal of the Society for Neuroscience. 1994; 14 (9):5160–9.

112. Warmke JW, Reenan RA, Wang P, Qian S, Arena JP, Wang J, et al. Functional expression of Drosophila para sodium channels. Modulation by the membrane protein TipE and toxin pharmacology. The Journal of general physiology. 1997; 110(2):119–33. https://doi.org/10.1085/jgp.110.2.119 PMID: 9236205

113. Mu L, Ito K, Bacon JP, Strausfeld NJ. Optic glomeruli and their inputs in Drosophila share an organizational ground pattern with the antennal lobes. The Journal of neuroscience: the official journal of the Society for Neuroscience. 2012; 32(18):6061–71.

114. Juusola M, Uusitalo RO, Weckstrom M. Transfer of graded potentials at the photoreceptor-interneuron synapse. The Journal of general physiology. 1995; 105(1):117–48. https://doi.org/10.1085/jgp.105.1.117 PMID: 7537323

115. Uusitalo RO, Juusola M, Kouvalainen E, Weckstrom M. Tonic transmitter release in a graded potential synapse. Journal of neurophysiology. 1995; 74(1):470–3. https://doi.org/10.1152/jn.1995.74.1.470 PMID: 7472349

116. Stenesen D, Moehlman AT, Schellinger JN, Rodan AR, Kramer H. The glial sodium-potassium-2-chloride cotransporter is required for synaptic transmission in the Drosophila visual system. Scientific reports. 2019; 9(1):2475. https://doi.org/10.1038/s41598-019-38850-x PMID: 30792494

117. Weckstrom M, Laughlin S. Extracellular potentials modify the transfer of information at photoreceptor output synapses in the blowfly compound eye. The Journal of neuroscience: the official journal of the Society for Neuroscience. 2010; 30(28):9557–66.

118. Nikolaev A, Zheng L, Wardill TJ, O'Kane CJ, de Polavieja GG, Juusola M. Network adaptation improves temporal representation of naturalistic stimuli in Drosophila eye: II mechanisms. PloS one. 2009; 4(1):e4306. https://doi.org/10.1371/journal.pone.0004306 PMID: 19180195

119. Pyza E, Gorska-Andrzejak J. Involvement of glial cells in rhythmic size changes in neurons of the housefly's visual system. J neurobiol. 2004; 59(2):205–15. https://doi.org/10.1002/neu.10307 PMID: 15085538

120. Benna C, Bonaccorsi S, Wulbeck C, Helfrich-Forster C, Gatti M, Kyriacou CP, et al. Drosophila timeless2 is required for chromosome stability and circadian photoreception. Current biology: CB. 2010; 20 (4):346–52. https://doi.org/10.1016/j.cub.2009.12.048 PMID: 20153199

121. Coates KE, Majot AT, Zhang X, Michael CT, Spitzer SL, Gaudry Q, et al. Identified Serotonergic Modulatory Neurons Have Heterogeneous Synaptic Connectivity within the Olfactory System of Drosophila. The Journal of neuroscience: the official journal of the Society for Neuroscience. 2017; 37(31):7318–31.

122. Gaspar P, Lillesaar C. Probing the diversity of serotonin neurons. Philosophical transactions of the Royal Society of London Series B, Biological sciences. 2012; 367(1601):2382–94. https://doi.org/10.1098/rstb.2011.0378 PMID: 22826339

123. Herve D, Pickel VM, Joh TH, Beaudet A. Serotonin axon terminals in the ventral tegmental area of the rat: fine structure and synaptic input to dopaminergic neurons. Brain res. 1987; 435(1–2):71–83. https://doi.org/10.1016/0006-8993(87)91588-5 PMID: 2892580

124. Moukhles H, Bosler O, Bolam JP, Vallee A, Umbriaco D, Geffard M, et al. Quantitative and morphometric data indicate precise cellular interactions between serotonin terminals and postsynaptic targets in rat substantia nigra. Neuroscience. 1997; 76(4):1159–71. https://doi.org/10.1016/s0306-4522(96)00452-6 PMID: 9027876

125. Nässel DR, Elekes K. Ultrastructural demonstration of serotonin-immunoreactivity in the nervous system of an insect (Calliphora erythrocephala). Neurosci lett. 1984; 48(2):203–10. https://doi.org/10.1016/0304-3940(84)90020-x PMID: 6384830

126. Zheng Z, Lauritzen JS, Perlman E, Robinson CG, Nichols M, Milkie D, et al. A Complete Electron Microscopy Volume of the Brain of Adult Drosophila melanogaster. Cell. 2018; 174(3):730–43 e22. https://doi.org/10.1016/j.cell.2018.06.019 PMID: 30033368

127. Eckstein N, Bates AS, Du M, Hartenstein V, Jefferis GSXE, Funke J. Neurotransmitter Classification from Electron Microscopy Images at Synaptic Sites in Drosophila. BioRxiv. 2020:2020.06.12.148775.

128. Altieri SC, Garcia-Garcia AL, Leonardo ED, Andrews AM. Rethinking 5-HT1A receptors: emerging modes of inhibitory feedback of relevance to emotion-related behavior. ACS chem neurosci. 2013; 4 (1):72–83. https://doi.org/10.1021/cn3002174 PMID: 23336046

129. Andrade R, Huereca D, Lyons JG, Andrade EM, McGregor KM. 5-HT1A Receptor-Mediated Autoinhibition and the Control of Serotonergic Cell Firing. ACS chem neurosci. 2015; 6(7):1110–5. https://doi.org/10.1021/acschemneuro.5b00034 PMID: 25913021

130. Courtney NA, Ford CP. Mechanisms of 5-HT1A receptor-mediated transmission in dorsal raphe serotonin neurons. J physiol. 2016; 594(4):953–65. https://doi.org/10.1113/JP271716 PMID: 26634643

131. Freifeld L, Clark DA, Schnitzer MJ, Horowitz MA, Clandinin TR. GABAergic lateral interactions tune the early stages of visual processing in Drosophila. Neuron. 2013; 78(6):1075–89. https://doi.org/10.1016/j.neuron.2013.04.024 PMID: 23791198

132. Keles MF, Hardcastle BJ, Stadele C, Xiao Q, Frye MA. Inhibitory Interactions and Columnar Inputs to an Object Motion Detector in Drosophila. Cell rep. 2020; 30(7):2115–24 e5. https://doi.org/10.1016/j.celrep.2020.01.061 PMID: 32075756

133. Halberstadt AL. Recent advances in the neuropsychopharmacology of serotonergic hallucinogens. Behav Brain Res. 2015; 277:99–120. https://doi.org/10.1016/j.bbr.2014.07.016 PMID: 25036425

134. Li YH, Xiang K, Xu X, Zhao X, Li Y, Zheng L, et al. Co-activation of both 5-HT1A and 5-HT7 receptors induced attenuation of glutamatergic synaptic transmission in the rat visual cortex. Neurosci lett. 2018; 686:122–6. https://doi.org/10.1016/j.neulet.2018.09.013 PMID: 30205142

135. Sizemore TR, Dacks AM. Serotonergic Modulation Differentially Targets Distinct Network Elements within the Antennal Lobe of Drosophila melanogaster. Scientific reports. 2016; 6:37119. https://doi.org/10.1038/srep37119 PMID: 27845422

136. Gordon MD, Scott K. Motor control in a Drosophila taste circuit. Neuron. 2009; 61(3):373–84. https://doi.org/10.1016/j.neuron.2008.12.033 PMID: 19217375

137. Schindelin J, Arganda-Carreras I, Frise E, Kaynig V, Longair M, Pietzsch T, et al. Fiji: an open-source platform for biological-image analysis. Nature methods. 2012; 9(7):676–82. https://doi.org/10.1038/nmeth.2019 PMID: 22743772

138. Tan L, Zhang KX, Pecot MY, Nagarkar-Jaiswal S, Lee PT, Takemura SY, et al. Ig Superfamily Ligand and Receptor Pairs Expressed in Synaptic Partners in Drosophila. Cell. 2015; 163(7):1756–69. https://doi.org/10.1016/j.cell.2015.11.021 PMID: 26687360

139. Hu Y, Sopko R, Foos M, Kelley C, Flockhart I, Ammeux N, et al. FlyPrimerBank: an online database for Drosophila melanogaster gene expression analysis and knockdown evaluation of RNAi reagents. G3 (Bethesda). 2013; 3(9):1607–16.

140. Picelli S, Bjorklund AK, Faridani OR, Sagasser S, Winberg G, Sandberg R. Smart-seq2 for sensitive full-length transcriptome profiling in single cells. Nature methods. 2013; 10(11):1096–8. https://doi.org/10.1038/nmeth.2639 PMID: 24056875

141. Picelli S, Faridani OR, Bjorklund AK, Winberg G, Sagasser S, Sandberg R. Full-length RNA-seq from single cells using Smart-seq2. Nature protocols. 2014; 9(1):171–81. https://doi.org/10.1038/nprot.2014.006 PMID: 24385147

142. Dobin A, Davis CA, Schlesinger F, Drenkow J, Zaleski C, Jha S, et al. STAR: ultrafast universal RNA-seq aligner. Bioinformatics. 2013; 29(1):15–21. https://doi.org/10.1093/bioinformatics/bts635 PMID: 23104886

143. Keles MF, Frye MA. Object-Detecting Neurons in Drosophila. Current biology: CB. 2017; 27(5):680–7. https://doi.org/10.1016/j.cub.2017.01.012 PMID: 28190726

144. Stadele C, Keles MF, Mongeau JM, Frye MA. Non-canonical Receptive Field Properties and Neuromodulation of Feature-Detecting Neurons in Flies. Current biology: CB. 2020.

145. Weir PT, Dickinson MH. Functional divisions for visual processing in the central brain of flying Drosophila. Proceedings of the National Academy of Sciences of the United States of America. 2015; 112 (40):E5523–32. https://doi.org/10.1073/pnas.1514415112 PMID: 26324910

146. Wilson RI, Turner GC, Laurent G. Transformation of olfactory representations in the Drosophila antennal lobe. Science. 2004; 303(5656):366–70. https://doi.org/10.1126/science.1090782 PMID: 14684826

147. Akin O, Zipursky SL. Frazzled promotes growth cone attachment at the source of a Netrin gradient in the Drosophila visual system. Elife. 2016;5.